JOURNAL OF PETROLOGY | VOLUME 44 | NUMBER 7 | PAGES 1309–1344 | 2003

The Appinite–Migmatite Complex of Sanabria, NW Iberian Massif, Spain

ANTONIO CASTRO[1]*, L. GUILLERMO CORRETGÉ[2], JESÚS D. DE LA ROSA[1], CARLOS FERNÁNDEZ[3], SUSANA LÓPEZ[1], OLGA GARCÍA-MORENO[2] AND HELENA CHACÓN[1]

[1]DEPARTAMENTO DE GEOLOGÍA, UNIVERSIDAD DE HUELVA, CAMPUS DE EL CARMEN, 21071 HUELVA, SPAIN

[2]DEPARTAMENTO DE GEOLOGÍA, UNIVERSIDAD DE OVIEDO, JESUS ARIAS DE VELASCO S/N, 33005 OVIEDO, SPAIN

[3]DEPARTAMENTO DE GEODINÁMICA Y PALEONTOLOGÍA, UNIVERSIDAD DE HUELVA, CAMPUS DE EL CARMEN, 21071 HUELVA, SPAIN

RECEIVED SEPTEMBER 8, 2002; ACCEPTED FEBRUARY 27, 2003

The Sanabria appinitic rocks and host migmatites form an unusual, non-peri-batholithic complex in which all the typical members of the appinite suite are present. It differs from most appinitic complexes in the deeper level of emplacement and the close temporal and spatial association with migmatites. Consequently, many in situ *relationships that resulted from the invasion of mafic magma into a crustal anatectic zone are extremely well preserved. The complex shows unequivocal relations between members of the appinitic suite and between these and migmatites derived by anatexis of a gneissic formation (Ollo de Sapo gneiss). These relations point to derivation of monzodiorites and biotite diorites by hydrous basalt fractionation combined with fluid-assisted melting of the crustal rocks surrounding the appinitic intrusions. This hydrous basic magma may be derived from an enriched region of the mantle associated with subduction. Petrogenetic models have been tested using a combination of field relations and geochemical data. Despite the complexity of the processes involved, it is concluded that water played an important role in the petrogenesis of the intermediate and mafic magmas. Reaction between monzodiorite melts and the host migmatites was responsible for the generation of a range of intermediate rocks within the complex. The need for water to facilitate magma generation in both the mantle and the crust suggests that melting is linked with subduction. This interpretation has important implications because appinitic magmatism may be considered as indicative of subduction processes involved not only in the generation of the mafic end-members of the suite, but also in the generation of batholiths with which the appinitic rocks are spatially and temporally associated.*

KEY WORDS: *appinite; monzodiorite; migmatite; Variscan orogen; Iberian massif*

INTRODUCTION

One of the most significant features of late Caledonian and late Variscan granitoid batholiths within Europe is the close spatial and temporal association with mafic and ultramafic rocks of the so-called 'appinite suite' (Bailey, 1960). This suite includes several types of mafic rock characterized by hydrous mineral assemblages with hornblende and biotite and by an overall andesitic to basaltic composition of calc-alkaline affinity (French, 1966; Bowes & McArthur, 1976; Gil Ibarguchi, 1980, 1981; Sabatier, 1991; Galán *et al*., 1997; Pitcher, 1997). Some of these rocks can be included among the so-called 'basic precursors' (Capdevila, 1969) or 'mafic precursors' (Bea *et al*., 1999) of the batholiths and have been considered to represent some kind of mantle involvement in granitoid petrogenesis (e.g. Holden *et al*., 1987; Galán & Suárez, 1989). Geochemical and Nd–Sr isotopic relationships between these mafic rocks

*Corresponding author. E-mail: dorado@uhu.es

and the granitoids strongly suggest that they may be related by a petrogenetic process such as fractionation, assimilation or magma mixing (e.g. Fowler & Henney, 1996; Pitcher, 1997; Fowler *et al*., 2001). However, the intricacies of these petrogenetic processes remain poorly understood and many questions and paradoxes still are unsolved. The fact that most appinitic rocks appear as small peri-batholithic complexes and mega-enclaves transported by the enclosing granite makes it difficult to recognize their primary characteristics. It is reasonable to assume that a great part of the diversity of textures and compositions of the appinitic complexes resulted from deep-seated processes not recognizable at the level of emplacement. Paradoxically, the geochemical relationships indicate that mantle components, supposedly supplied by the appinitic magmas, were incorporated into the granites and, at the same time, crustal components are identified in the geochemical characteristics of the appinites (e.g. Bea *et al*., 1999). The way in which these interchanges took place is, however, poorly constrained. Magmatic fractionation, either by crystal accumulation or fluid migration, seems to be plausible to account for the variations in major elements. However, open-system processes, for example crustal assimilation, are required to account for the isotopic signatures (e.g. Fowler *et al*., 2001). Neither of these processes, fractionation or assimilation, is unambiguously evidenced by field relationships, as a result of the discontinuous and fragmented nature of the isolated outcrops that characterize most appinitic complexes.

The Sanabria complex, described in this paper, is not a typical transported or peri-batholithic appinitic complex. It differs from most appinitic complexes in the deeper level of emplacement and the close temporal and spatial association with migmatites. Consequently, many *in situ* relationships that resulted from the invasion of mafic magma into a crustal anatectic zone are preserved. Furthermore, the complete range of rock types that constitutes the appinitic suite is present in the Sanabria complex, showing original relationships between them on a scale of metres to kilometres. These relationships provide important information on the intricacies of the complex processes that gave rise to the textural and compositional diversity of the members of the appinitic suite. Geochemical and isotopic (Sr, Nd) data are also presented, with the aim of characterizing the Sanabria appinite suite and to make comparisons with similar complexes from elsewhere in the Caledonian and Variscan belts.

REGIONAL GEOLOGY

The Iberian massif is one of the largest exposures of the Variscan orogen in Europe. The northwestern part of the Iberian massif experienced the effects of the Variscan collision between the Palaeozoic continental margin of Gondwana and a complex mosaic of Laurentian terranes (Martínez Catalán *et al*., 1997). As a consequence of this tectonic history, a number of tectonothermal processes took place in the northern Iberian massif at the end of the Palaeozoic, including syn-tectonic igneous activity and high-temperature metamorphism. The internal zonation of the Iberian massif (e.g. Julivert *et al*., 1974) is a result of the stratigraphical, structural and petrological evolution of this part of the Variscan orogen. The Sanabria area is located at the boundary between two major domains of the Iberian massif: the West Asturian–Leonese Zone (WALZ) and the Central Iberian Zone (CIZ) (Fig. 1a). The boundary coincides with a large structure, the Ollo de Sapo Anticlinorium, which is characterized by the presence of a thick sequence (1500–2000 m) of augen-gneisses (Ollo de Sapo gneiss) (Fig. 1b) of Early Ordovician age (Gebauer *et al*., 1993; Valverde & Dunning, 2000), which appear to be derived from an original volcanoclastic protolith (Navidad, 1979; Ortega, 1998).

GEOLOGY OF THE SANABRIA AREA

The Ollo de Sapo gneisses in the Sanabria region were intruded by basic magmas during the early stages of the tectonothermal evolution of the region (Variscan Orogeny), producing a wide variety of rock types with complex field relationships (Fig. 2). These mafic rocks and their host migmatites are the subject of this study. Three main deformation phases affected the Ollo de Sapo gneisses in Sanabria (Díez Balda *et al*., 1990). The large-scale structure is the result of superposed folding. D_1 deformation gave rise to a first generation of NE-verging, recumbent folds, which have an associated axial-plane foliation (S_1). The entire Sanabria region (Fig. 1b) is located in the normal limb and hinge of a large recumbent D_1 fold, with the Ollo de Sapo gneisses located in the middle to lower part of this fold limb (Arias *et al*., 2000). Two facies can be recognized in the Ollo de Sapo area and surroundings (Martínez García, 1969)—a lower augen-gneiss, overlain by a fine-grained facies (Fig. 1b). Fine-grained gneisses are covered by metasediments ranging in age from Lower Ordovician to Devonian. A second planar–linear fabric (S_2 and L_2) is observed in the augen-gneisses. S_2 varies gradually from a crenulation cleavage affecting S_1 in the fine-grained gneisses, to a schistosity in the basal augen-gneisses, where it penetrates the whole rock and transposes the previous S_1 fabric. A concomitant increase in the metamorphic grade is observed from top to bottom in the Ollo de Sapo gneisses. The D_2 deformation is interpreted as

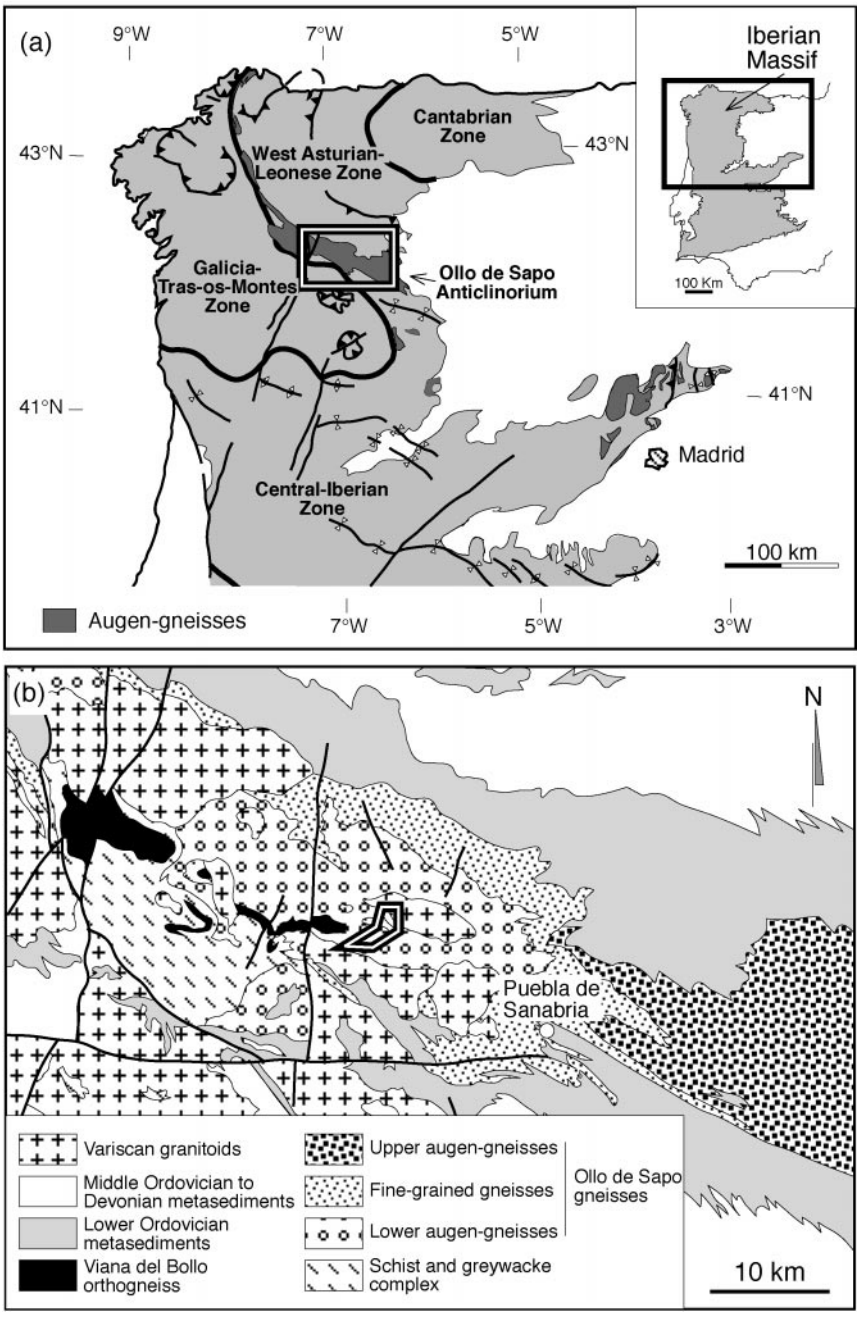

Fig. 1. (a) Location of the Sanabria area in the Iberian massif. (b) Geological sketch of the Ollo de Sapo Anticlinorium in the Sanabria region [modified after Lancelot *et al.* (1985)]. The rectangle in (a) shows the location of the study area. The polygon in (b) corresponds to the area studied in detail, illustrated in Fig. 2.

due to an intense subhorizontal shearing. The observed kinematic criteria indicate a top-to-the-SE sense of movement for this shear zone, acting as an extensional structure. Migmatization of the basal Ollo de Sapo augen-gneisses coincides with the D_2 shearing, and affected the core and deepest parts of the D_1 recumbent fold. This is the specific area studied here (Fig. 2), where the D_1 structures are almost completely transposed by D_2. The last deformation phase (D_3) is responsible for a second generation of folds. These are kilometre-scale, sub-cylindrical, upright and north-verging folds, with subrounded to sub-angular closures (Twiss, 1988). Vegas *et al.* (2001) interpreted the D_3 folds at a regional scale as formed in association with a dextral strike-slip fault stepover. Intrusion of mafic and intermediate igneous rocks in

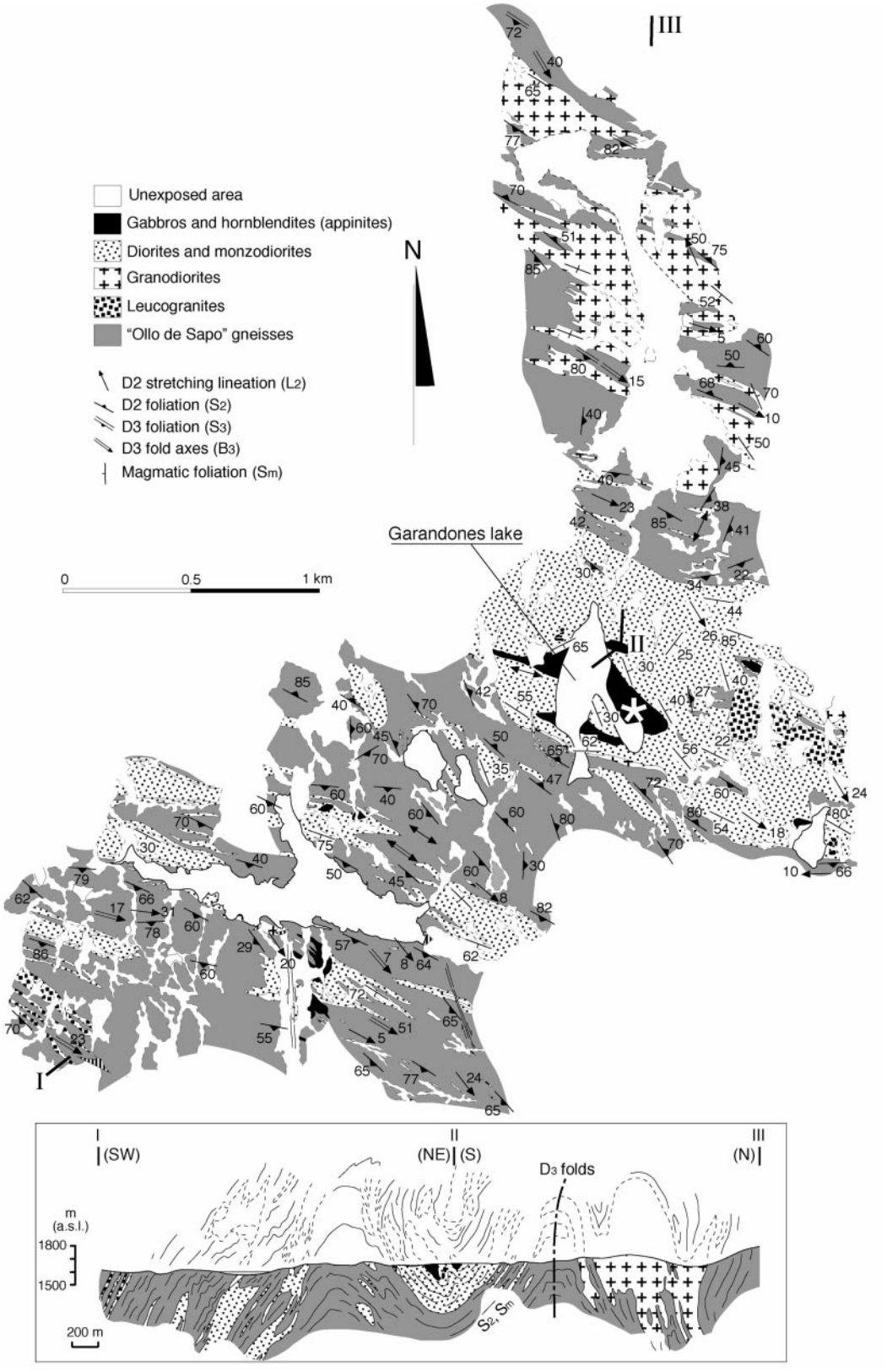

Fig. 2. Geological map and cross-section of the Sanabria area according to data obtained in this study, showing the main field relationships between migmatites, basic rocks and granitoids. White asterisk indicates the outcrop location illustrated in detail in Fig. 7.

Sanabria is syn-kinematic with D_2 deformation and with the migmatization of the Ollo de Sapo host gneisses. Therefore, knowledge of this tectonic sequence is essential to understand the petrogenetic processes involved. Absolute age determinations yield an age within the range 340–350 Ma (Dallmeyer *et al.*, 1997, and references therein) for the D_2 deformation and, hence, for the migmatization of the Ollo de Sapo gneiss. Consequently, a reference age of 345 Ma is used for corrections of initial isotopic ratios for Sr and Nd.

ROCK TYPES AND FIELD RELATIONS IN THE SANABRIA COMPLEX

Rock types and petrography

It is inferred from field relations observed in the Sanabria massif that some kind of interaction between mafic magmas and the Ollo de Sapo gneisses occurred at the level of emplacement. As noted above, the complex is not a classical peri-batholithic type, transported by granodiorite magmas from deep crustal zones (Castro *et al.*, 2002*a*). Consequently, it is expected that many of the observed field relations are primary, not modified by transportation from depth, and resulted from *in situ* processes related to the intrusion of mantle-derived magmas into anatectic rocks. The absence of radiometric ages for the mafic rocks precludes a precise chronology of events. Field relationships indicate that migmatization was coeval with the intrusion of the basic magmas in Sanabria. However, a cause-and-effect relation between the two processes cannot be established from this observation. In this paper we describe the most outstanding of these features because they have important implications for the formulation of petrogenetic hypotheses in relation to the generation of the varied spectrum of rocks of the appinitic suite. Appinite suite rocks, ranging in composition from hornblende gabbro to monzodiorite, are found in the Sanabria complex in an area about 3 km wide, extending for several kilometres along the regional trend of the tectonic structures. Detailed field relationships in an area of the Sanabria Natural Park between the Porto Lake and the Vegadetera Lake are shown in Fig. 2. This varied spectrum of rock compositions and textures is a general feature of appinitic complexes (see Pitcher, 1997).

To simplify the descriptions we have grouped all the rocks of the Sanabria complex into the following lithological groups: (1) hornblende gabbros and diorites; (2) monzodiorites; (3) banded diorites; (4) granodiorites; (5) leucogranites; (6) gneisses and migmatites. Although granodiorites and leucogranites form separate intrusions in the Sanabria area, they are included in this study because they are spatially associated with the mafic complexes and migmatites on a regional scale. Many appinitic mafic–ultramafic complexes in the Iberian Variscan massif are associated with granodiorite intrusions as peri-batholithic complexes (Castro *et al.*, 2002*a*).

Electron microprobe analyses of the main mineral phases, biotite, amphibole and plagioclase, were obtained from each of these lithological types. Biotites from a suite of samples from a traverse across a gabbro–monzodiorite contact in the Garandones area were also selected for electron probe microanalysis, performed using a Cameca Camebax SX-50 system equipped with four spectrometers at the University of Oviedo. Operating conditions were 15 kV accelerating potential and 15 nA probe current. Calibration standards are albite for Na, Si and Al; wollastonite for Ca and Si; NiO for Ni; corundum for Al; Cr_2O_3 for Cr; andradite for Fe and Ca; $MnTiO_3$ for Mn; periclase for Mg; orthoclase for K; magnetite for Fe; apatite for P. Data corrections are according to Pouchou & Pichoir (1984). Representative data are listed in Table 1.

Hornblende gabbros and diorites

These are coarse-grained rocks composed dominantly of hornblende and plagioclase. Hornblende gabbros (80–90 vol. % amphibole) occur as decametre-sized blocks and smaller enclaves surrounded by massive diorite and monzodiorite. An interesting feature is the presence of monzodiorites separating hornblende gabbro bodies and migmatites. Gabbros and migmatites are never found in direct contact. Patches of hornblendite (>90 vol. % amphibole), tens of metres in diameter, are found in the inner parts of the hornblende gabbro bodies. Hornblende gabbros and monzodiorites commonly appear as brecciated blocks intruded by leucotonalites and granitic veins (Fig. 3a). These hornblendites and hornblende gabbros are typically coarse-grained, hypidiomorphic rocks with cumulate-like texture (Fig. 3b). The contacts with the surrounding monzodiorites are sharp on a centimetre scale and often have lobate and crenulated shapes, suggestive of liquid–liquid contacts. In places the contact is back-veined and fragments of the hornblende gabbro bodies are completely incorporated to the surrounding monzodiorite (Fig. 3c). Partially digested blocks of the hornblende gabbro occur within the monzodiorites, ranging in size from clots of hornblende crystals up to a few centimetres in diameter. Another characteristic feature of the hornblende gabbros and the diorites is the presence of granitic enclaves (Fig. 3d) with rounded shapes, and ranging in size from a few centimetres to 0·5 m. These normally have a hornblende-rich outer margin suggesting

Table 1: Representative analyses of biotite and amphibole of the Sanabria complex

	Biotite									Amphibole		Biotite (Garandones profile)					Phlogopite		
Sample:	A59918	A59911	A119847	A59910	GC2559901	A59921	A109811	A11984	GC285991	A59918	A59910	H90144	H90145	H9018	H9019a	H90111	H90112	H90113	H90114
Rock type:	Gb	Mzd	Mzd	Dt	Gd	Mig	OSG	Gr	L2 Leu	Gb	Dt	Mzd	Mzd	Mzd	Mzd	Gb	Gb	Gb	Gb
SiO_2	38·32	38·10	37·20	36·76	35·99	35·37	35·23	34·94	35·46	51·96	48·78	36·25	36·33	37·28	37·34	37·41	39·39	39·58	39·21
TiO_2	3·13	2·02	3·17	4·55	3·52	4·55	3·17	2·91	2·85	0·39	0·72	3·44	3·14	3·43	2·86	2·85	1·81	2·35	1·73
Al_2O_3	15·09	16·86	16·11	15·91	17·11	18·56	18·09	18·20	17·32	4·84	7·56	16·09	16·92	16·66	15·58	14·91	15·32	15·40	15·03
FeOt	15·36	14·35	19·18	16·63	20·69	18·43	22·50	26·72	21·84	11·86	12·75	17·83	17·50	13·84	13·63	13·65	12·51	12·35	11·11
MnO	0·27	0·25	0·24	0·21	0·32	0·27	0·25	0·37	0·31	0·34	0·41	0·19	0·00	0·00	0·00	0·00	0·17	0·10	0·10
MgO	14·05	14·32	11·66	10·87	8·44	8·20	8·59	5·93	8·41	15·38	13·54	11·02	11·10	14·41	14·66	15·07	16·39	17·00	17·05
CaO	0·02	0·11	0·02	0·00	0·00	0·14	0·00	0·00	0·00	13·37	12·65	0·06	0·00	0·00	0·00	0·00	0·00	0·00	0·00
Na_2O	0·15	0·09	0·16	0·10	0·07	0·13	0·07	0·07	0·03	0·52	0·63	0·09	0·00	0·00	0·36	0·00	0·28	0·35	0·13
K_2O	9·75	9·82	9·54	10·60	10·19	9·41	9·18	8·90	9·65	0·34	0·57	9·28	9·13	8·97	8·61	8·61	9·56	8·49	9·18
Total	96·14	95·92	97·28	95·63	96·33	95·06	97·08	98·04	95·87	99·00	97·61	94·24	94·12	94·59	93·04	92·50	95·42	95·62	93·53
$Mg/(Mg + Fe_t^{2+})$	0·48	0·64	0·38	0·40	0·29	0·31	0·28	0·18	0·28	0·56	0·51	0·52	0·53	0·65	0·66	0·66	0·70	0·71	0·73

Operating conditions: accelerating voltage of 15 kV, beam intensity of 15 nA, and 10 s peak and 5 s background of counting time, with a beam size of 2 μm. Standards used for the analyses: albite for Na, Si and Al; wollastonite for Ca and Si; Al_2O_3 for Al; andradite for Fe and Ca; MgO for Mg; orthoclase for K; Fe_2O_3 for Fe. Precision was ±0·5% for all elements. Gb, gabbro; Mzd, monzodiorite; Dt, diorite; Gd, granodiorite; Mig, migmatite; OSG, Ollo de Sapo gneiss; Gr, granite; Leu, leucosome.

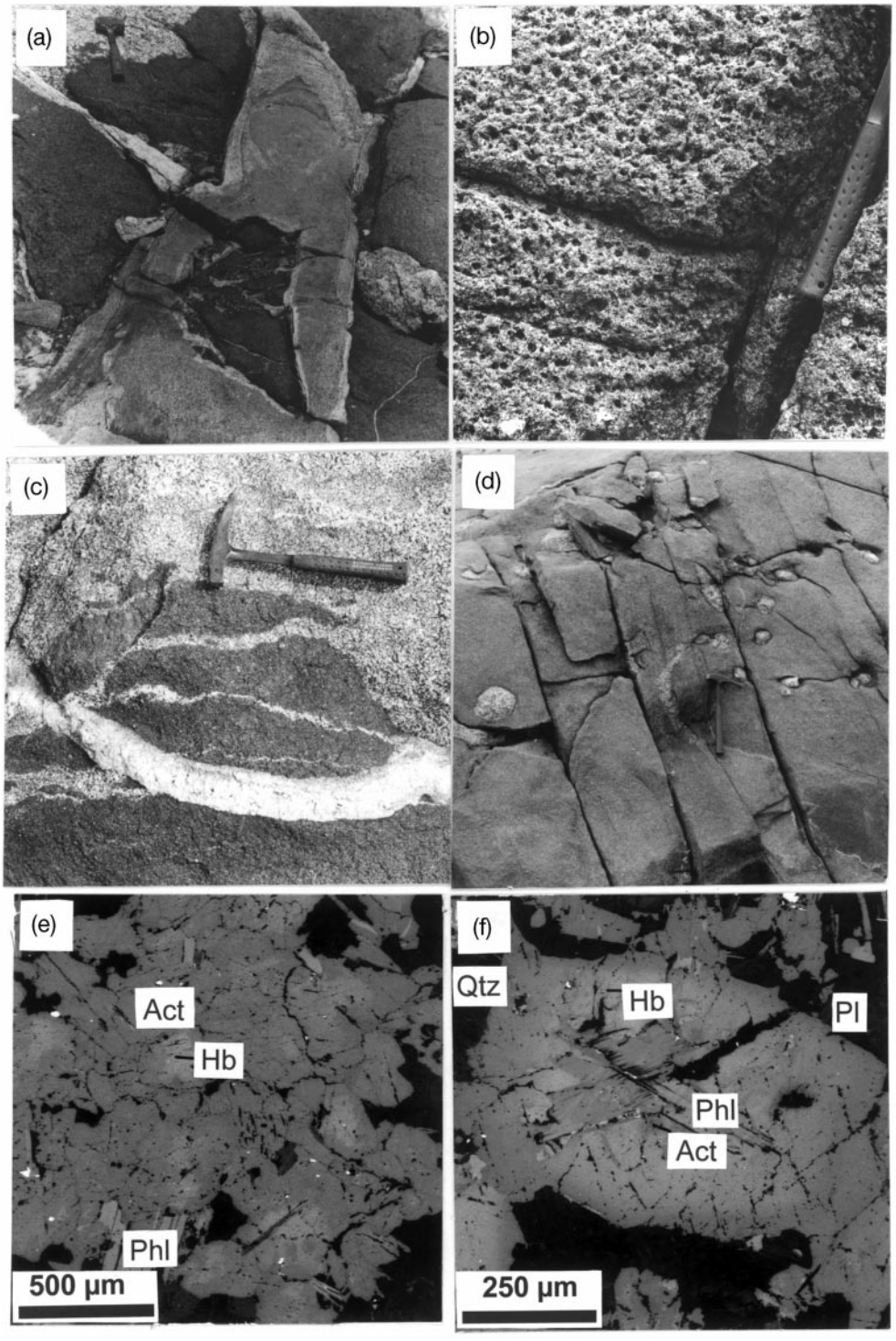

Fig. 3. Representative field relations and textural details of gabbroic rocks of the Sanabria complex. (a) Polygonal blocks of hornblende gabbro (darker) and monzodiorite (upper left corner) enclosed by leucocratic granitic veins. Sample location indicated in Fig. 7. (b) Typical field aspect of hornblende gabbros; the dark spots of 1 cm diameter are holes left after weathering of biotite and hornblende clots. (c) Detail of the contact between the hornblende gabbros (dark grey) and surrounding monzodiorites (pale grey); the grain size of the gabbro is finer near the contact and portions of this marginal zone are enclosed by the host monzodiorite. Sample location indicated in Fig. 7. (d) Granitic enclaves within the hornblende gabbro. (e) Backscattered electron image of an amphibole clot surrounded by Bt; the most typical textural feature of appinitic gabbros. (f) Euhedral hornblende (Hb) crystal of the Hb-gabbro with a biotite inclusion in the core; this textural relation between early biotite and late euhedral amphibole is very common in the appinitic gabbros.

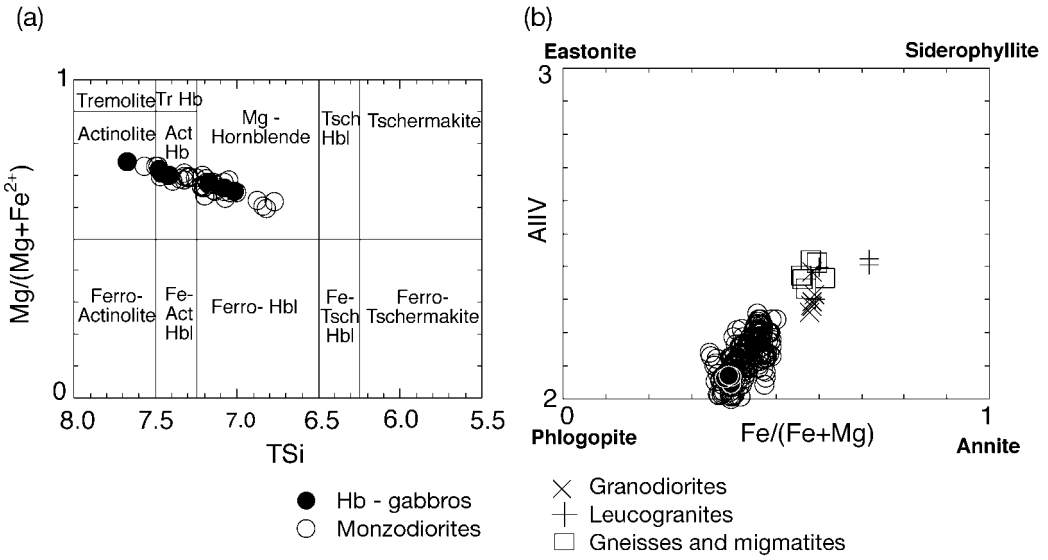

Fig. 4. Classification diagrams for amphiboles (a) and biotites (b) in the Sanabria appinites and migmatites.

some reaction between the granite enclaves and the host magma.

The most common medium-grained hornblende gabbros and diorites comprise amphibole (hornblende), plagioclase (An_{57}) and biotite. Similar to other hornblende-rich rocks of the appinitic suite, the hornblende gabbros of Sanabria typically contain polycrystalline clots of amphibole (Castro & Stephens, 1992; Stephens, 2001) surrounded by Mg-rich biotite rims (Fig. 3e). In particular, in the more silica-rich rock types (diorites and monzodiorites) the amphibole forms large (2–10 mm), euhedral crystals with a more Mg-rich core compared with the rim. These euhedral crystals are characterized by the presence of biotite inclusions (Fig. 3f). Accessory minerals are mainly apatite, titanite and Fe–Ti oxides. A diagnostic feature is the presence of poikilitic Mg-rich biotite with Mg-number = 0·6 [Mg-number = mol MgO/(mol MgO + mol FeO)] (Table 1). Amphiboles are classified (Leake, 1978) as Mg-hornblende to actinolite (Fig. 4a). Pargasite substitution is dominant, but Ti-Tschermak substitution is also observed. Compositional zoning in the amphibole crystals is common. Typically, cores are richer in total Al and depleted in Mg-number relative to rims. Chemical analyses of biotites are projected into Al^{IV} vs Fe/(Mg + Fe) composition space in Fig. 4b (Deer *et al.*, 1966).

Monzodiorites

These are medium- to fine-grained rocks composed of granular aggregates of plagioclase and amphibole, with subordinate biotite (Mg-number = 0·4), quartz and alkali feldspar. Plagioclase is highly variable in composition ($An_{26–64}$). Accessory minerals are titanite, zircon and apatite. Alkali feldspar occurs as large poikilitic crystals that include biotite and plagioclase.

This group of rocks is the most abundant of all the mafic and intermediate rocks in the Sanabria complex. Commonly, these rocks show mottled textures in which several plagioclase crystals are clustered around a partially resorbed titanite core. They also appear surrounding the bodies of hornblende gabbro and diorite as mentioned above. Near the contacts with these mafic bodies, the monzodiorites are very heterogeneous both in texture and composition. In close proximity to the gabbro they are locally coarse grained and have a pegmatitic appearance with large biotite crystals up to a few centimetres length. They also may contain irregular patches of plagioclase-rich rocks, interpreted as cumulates (Fig. 5a), which have intergranular biotite. These patches, together with the presence of hornblende gabbro enclaves (Fig. 5b) and partially disaggregated patches of migmatite (Fig. 5c), give these rocks a typically heterogeneous appearance. The study of these heterogeneities is of great interest in the formulation of petrogenetic models.

Banded diorites

This family of dioritic rocks are medium grained and typically have hypidiomorphic textures, consisting mainly of plagioclase (An content up to 59 mol %), biotite (Mg-number = 0·4) and amphibole, with accessory titanite, apatite, zircon and opaque minerals. Biotite generally encloses polycrystalline aggregates of Mg-hornblende. The diorites usually show a fine-scale banding (1–10 cm thick) defined by differences in grain

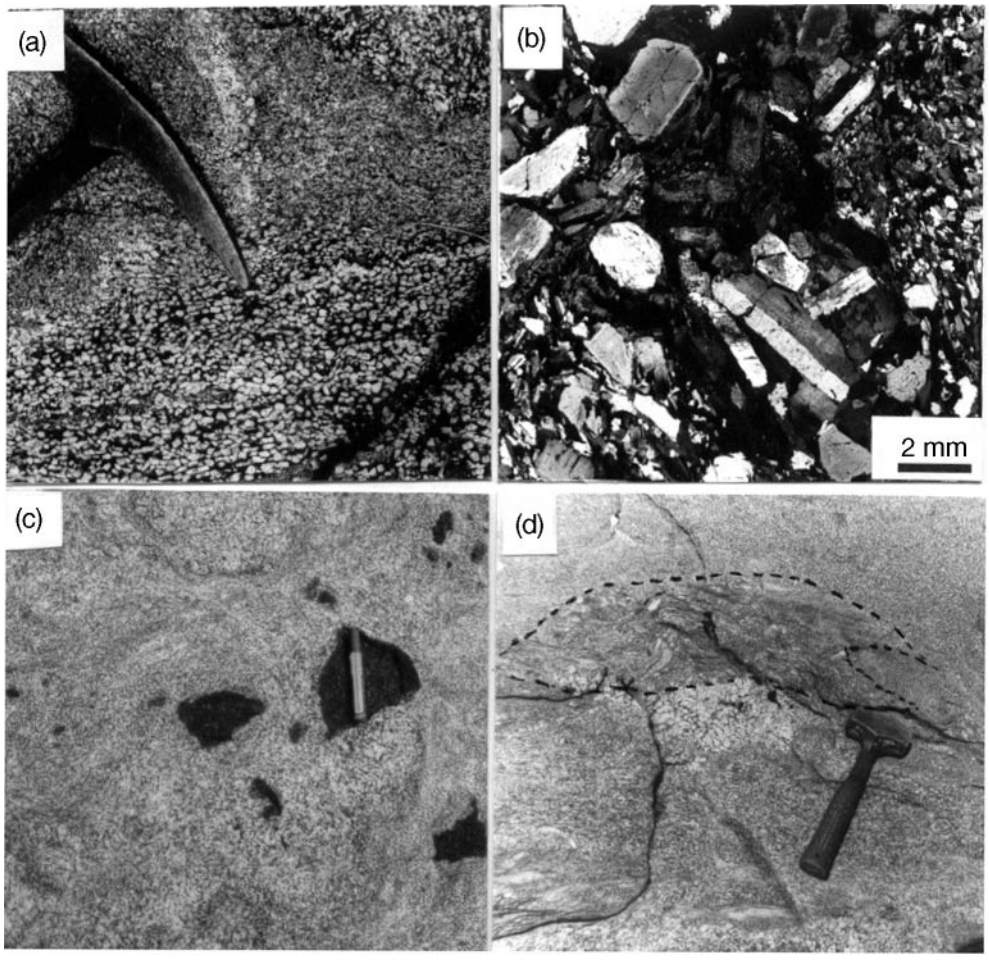

Fig. 5. Mesoscopic and microscopic aspects of heterogeneities that characterize the monzodiorites in the vicinities of the Hb-gabbro bodies. (a) Plagioclase cumulates forming irregular patches surrounded by finer-grained monzodiorite. (b) Detailed texture of these cumulates with intercumulus biotite. (c) Partially disaggregated enclaves of Hb-gabbro within the heterogeneous monzodiorite. Sample location indicated in Fig. 7. (d) Fragment of Ollo de Sapo migmatite gneiss, which is almost digested within the monzodiorite. The large K-feldspar megacrysts that characterize the Ollo de Sapo gneiss are still recognizable. A patch of plagioclase cumulate can be observed below the migmatite enclave (lighter patch in the centre, to the left of the hammer). Sample location indicated in Fig. 7.

size, with minor compositional changes in major elements (Fig. 6a). Plagioclase shows a trachytic texture (Fig. 6b) produced by magmatic flow parallel to the mesoscopic banding. Some bodies of banded diorite crop out in areas within the migmatized Ollo de Sapo gneisses, with which they are normally intercalated on a scale of centimetres (Fig. 6c), forming continuous bands parallel to the main foliation of the migmatized gneisses.

Granodiorites

Granodiorites form intrusive plutonic bodies in the northern part of the massif. They are coarse-grained rocks, typically with K-feldspar megacrysts. The main mineral phases are alkali feldspar, quartz, biotite (Mg-number = 0·3) and plagioclase (An_{37}), with zircon, titanite and apatite as accessory minerals. Some fine-grained, decametre-sized, tonalite bodies are found with these granodiorites.

Leucogranites

Leucogranites form irregular pockets (1–100 m) surrounded by migmatized gneisses (Ollo de Sapo) in several sectors of the Sanabria complex. They have hypidiomorphic textures and a medium grain size. Alkali feldspar is the main mineral phase together with quartz and plagioclase (An_{10}). Biotite (Mg-number = 0·2) and muscovite are scarce and interstitial. Accessory minerals are apatite and zircon.

Gneisses and migmatites

The Ollo de Sapo gneisses are coarse-grained rocks with porphyroblastic textures made up of K-feldspar

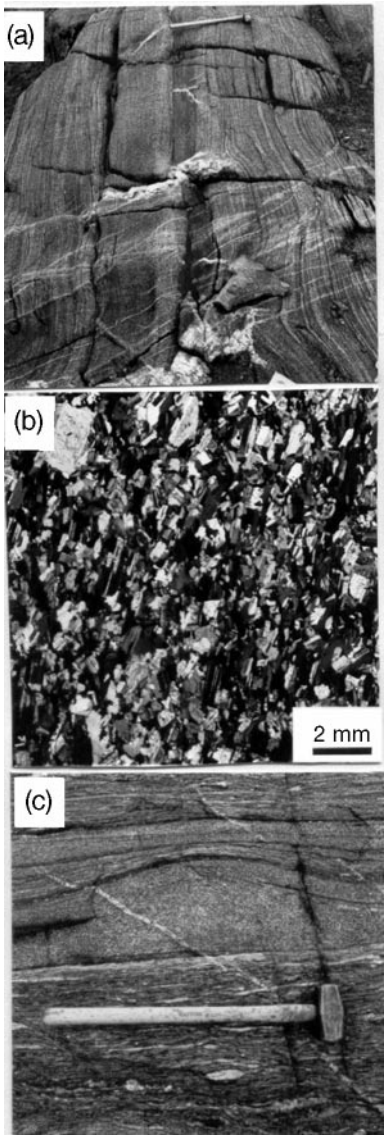

Fig. 6. Details of the magmatic layering that characterizes the banded diorites of the Sanabria complex. (a) Field aspect of the fine magmatic layering defined by alternating darker and lighter bands of variable width from 1 to 20 cm; compositional differences are minor between the dark and light bands. Most differences are in the grain size. (b) Microscopic aspect of this magmatic layering (note the trachytic texture defined by the orientation of plagioclase laths). (c) Diorite bands (grey) intercalated within the Ollo de Sapo migmatites. The bands are subparallel to the main foliation of the migmatitic gneiss but no foliation is observed within the diorite.

megacrysts, quartz, plagioclase and biotite (Mg-number = 0·3). Alkali feldspar megacrysts can be up to 10 cm in length, and can have inclusions of quartz, biotite, apatite and plagioclase. Some fibrolite crystals have been found in the migmatized facies of the gneisses. Zircon and apatite are the main accessory minerals. Leucosomes occur as veins, or elongated lenses either following the foliation in the migmatized gneisses or filling up shear zones and extensional structures and veins. The leucosomes are similar to the leucogranites, and have alkali feldspar as the main mineral phase, with quartz and Na-rich plagioclase ($An_{0–11}$). Some muscovite and biotite are always present.

Mutual relationships and implications

Hornblende-rich gabbros and intermediate rocks crop out as massive blocks showing a concentric zoning with more mafic rocks at the centre, surrounded by diorites and monzodiorites. These intermediate rocks also occur as foliated tabular or lensoidal layers, ranging in thickness from a few centimetres to more than 100 m, alternating with migmatized gneisses at the periphery of these zoned mafic bodies.

Monzodioritic rocks show a fine-scale layering defined by alternating bands (Fig. 6a), on a centimetre scale, with differences in grain size but not of chemical composition. There is a marked mineral foliation in these bands defined mainly by the orientation of plagioclase laths (Fig. 6b) and biotite flakes. Interstitial quartz is not deformed and there is no intracrystalline deformation in plagioclase. Therefore, and according to the criteria outlined by Paterson *et al*. (1989), this mineral foliation is considered as magmatic in origin. In the peripheral regions, surrounding the main mafic complex, monzodiorites and tonalites appear as small rafts within the leucosomes of the migmatized gneiss. These monzodiorites and tonalites do not show any sign of solid-state internal deformation and they are interpreted as the remains of dismembered synplutonic dykes injected at an early stage into the partially molten migmatite. The orientation of biotite aggregates and elongated leucosomes define the S_2 foliation in the migmatized gneisses. A remarkable observation is the absence of solid-state deformation microstructures in the leucosomes of the migmatized gneisses, which have a granular, hypidiomorphic microstructure and alternate in banded complexes with monzodiorite–tonalite layers (Fig. 6c). S_2 and S_m (magmatic foliation) are parallel at both outcrop and map scales (Fig. 2). Kinematic criteria associated with S_m in the monzodiorites and tonalites include a weak mineral lineation, folds and shear bands that indicate a shear sense consistent with that observed in the migmatites. The inference from these observations is that migmatites and monzodiorite–tonalite bands were deformed in the magmatic state, one as an anatectic system (migmatites) and the other as a crystallizing magma (monzodiorite–tonalite bands). S_2 and S_m are a consequence of the same D_2 shearing event, and were subsequently folded by D_3. Therefore, the intrusion of

the mafic magmas and the migmatization of the Ollo de Sapo gneiss were coeval.

Granodiorites form large bodies in the northern part of the mapped area. They were emplaced in lateral continuity with the main mafic complex (see cross-section in Fig. 2). Granodiorites always appear intercalated with migmatized gneisses and both have complex geometric relationships at the scale of the map.

From these relations it seems clear that some kind of physical and possibly chemical interaction between the appinitic magmas and the migmatites is likely to have occurred at the level of intrusion into the anatectic zone. The zonal distribution of mafic and intermediate rocks of the appinitic suite and the syn-kinematic and syn-anatectic character of the intrusions clearly indicate that interaction took place at this level of the crust and that the observed relations are *in situ*. This is important because it allows us to investigate the processes involved in the generation of hybrid magmas. Detailed information about these processes can be obtained from the relations observed in the Garandones Lake area, at the core of the zoned complex.

Small-scale field relations in the Garandones Lake area

Good exposures in the Garandones Lake area, at the core of the main mafic body (Fig. 2) supply important information on the relations between the various members of the appinitic suite. Figure 7 shows a detailed map of a 40 m × 15 m outcrop in which the relations between hornblende gabbros and intermediate rocks are clearly exposed. The inset to this map shows the locations of samples obtained across a boundary between hornblende gabbros and monzodiorites. Appinites *sensu stricto* (hornblende gabbros and diorites) and hornblendites occur as brecciated blocks within leucocratic monzodiorites and quartz diorites. These composite bodies were later brecciated and back-veined by a network of leucocratic veins. Some partially dismembered blocks of gneiss are included in the diorites. Hornblende gabbros, with typical poikilitic Mg-biotite and Mg-hornblende, are the dominant rocks at the core of the zoned complexes. Plagioclase cumulates with interstitial biotite also appear as isolated blocks enclosed within the diorites. Hornblende gabbros may contain rounded granitic inclusions surrounded by a reaction rim rich in amphibole. These inclusions are also present at the scale of individual crystals of quartz showing the same amphibole-rich rim, similar to the ocellar structures frequently found in microgranular enclaves and intermediate rocks of the appinitic suite (Vernon, 1983, 1991). These granitic inclusions may represent portions of granitic rocks that were incorporated by the basic magma during intrusion into the continental crust. This interpretation is supported by the presence of reaction rims around these granitic inclusions, indicating that they were in disequilibrium and were partially dissolved by the host mafic magma.

Another important observation in the outcrops of the Garandones area is that hornblende gabbros are surrounded by a discontinuous marginal facies of pegmatitic diorite (Fig. 2) composed of large crystals (>1 cm) of biotite intergrown with plagioclase. Some quartz is also present in these dioritic pegmatites. Large fragments of the partially molten Ollo de Sapo migmatites appear disaggregated and partially digested within the monzodioritic rocks surrounding the hornblende gabbros. In places, only the large K-feldspar megacrysts from the migmatized Ollo de Sapo gneiss are identifiable. The matrix is composed of a leucocratic diorite, instead of the typical granite. Plagioclase in these intermediate rocks exhibits complex zoning patterns resulting from disequilibrium processes related to changes in magma composition (Castro, 2001). The inference from these observations is that some chemical reaction must have taken place between the water-rich mafic magma (the monzodioritic pegmatite) and the partially molten migmatite. These field observations are crucial to understand the complex chemical relationships found between the rock types within the Sanabria complex. In particular, the observations on the transition from hornblende gabbro to diorite are considered in some detail below so as to decide whether the gabbros represent magmatic cumulates or mafic restites left behind after partial melting.

Samples from a profile across the contact between the hornblende gabbro and diorite have been studied in detail in a block 1 m × 3 m in diameter, which is intruded by leucocratic veins (Fig. 7). The rocks on both sides of the interface show gradual changes in texture, grain size and modal composition, suggesting that the contact is primary and related to the magmatic evolution of both magmatic systems. In detail, the contact between hornblende gabbro and biotite-rich pegmatitic monzodiorite is irregular, but sharp at the scale of individual crystals. Near the contact, portions of the hornblende gabbro are incorporated as enclaves into the monzodiorite. The grain size of the monzodiorite is coarser at the contact with the hornblende gabbro and decreases away from it. In the hornblende gabbro, the grain size and hornblende content show some variations from the contact towards the interior of the block. The grain size is finer and the biotite content higher within a narrow 0·3–1·0 m band near the contact with the monzodiorite. The pegmatitic texture with large biotite crystals (up to 2 cm) and

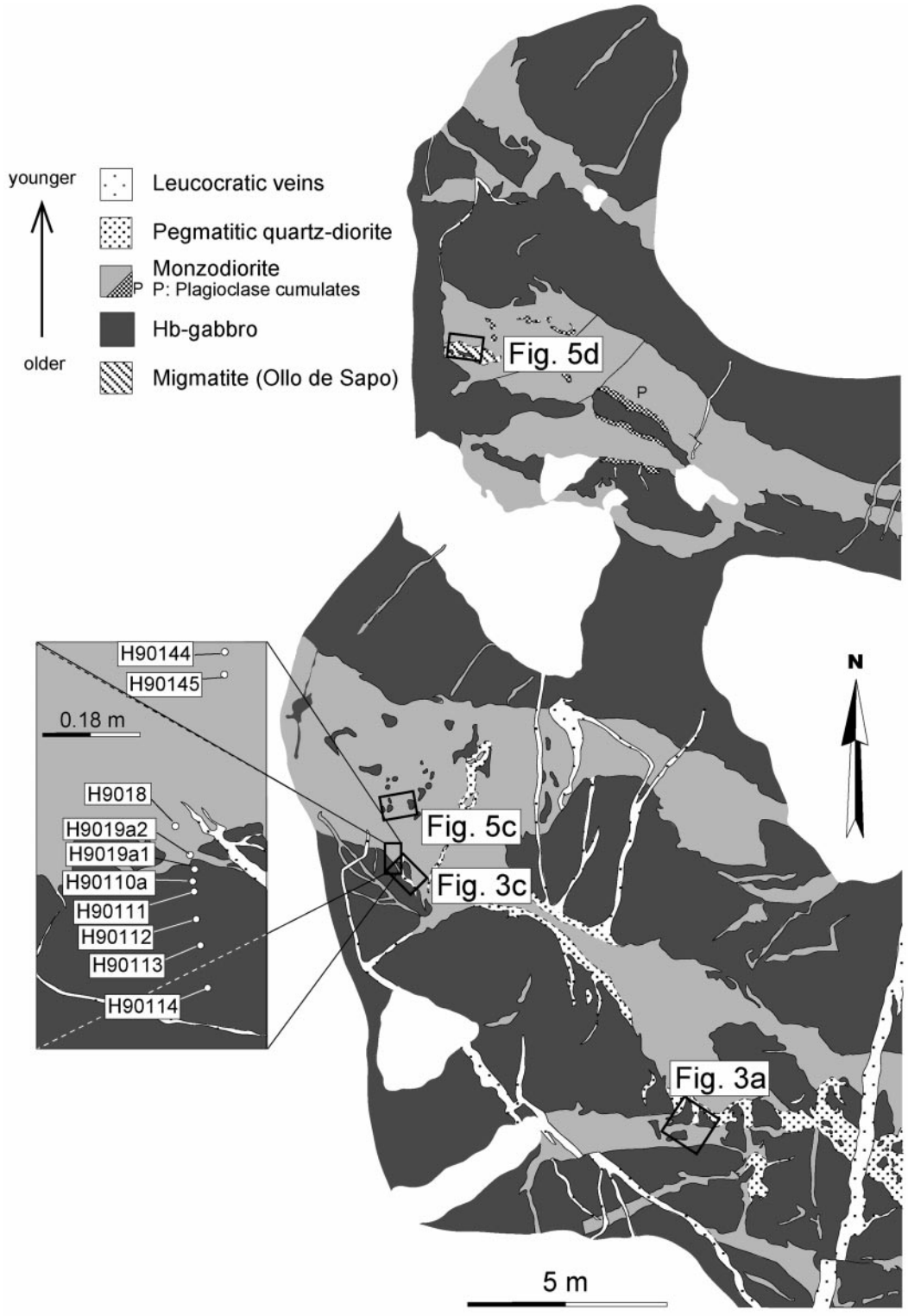

Fig. 7. Geological sketch map of a representative outcrop of the Garandones Lake area showing the detailed field relationships between Hb-gabbros and diorites. The gabbros form large brecciated blocks within a monzodiorite host that are back-veined by leucocratic veins of granite to tonalite composition. The leucocratic veins and pegmatitic monzodiorites are transitional facies. The Hb-gabbro is back-veined by residual melts from the dioritic magma that surrounded the gabbro intrusion. The curved and irregular shapes of the contacts between the gabbros and monzodiorites indicate the magma–magma nature of these contacts. The inset shows a detail of the Garandones profile with the location of samples studied for geochemistry and mineral composition across the contact between Hb-gabbro and monzodiorite.

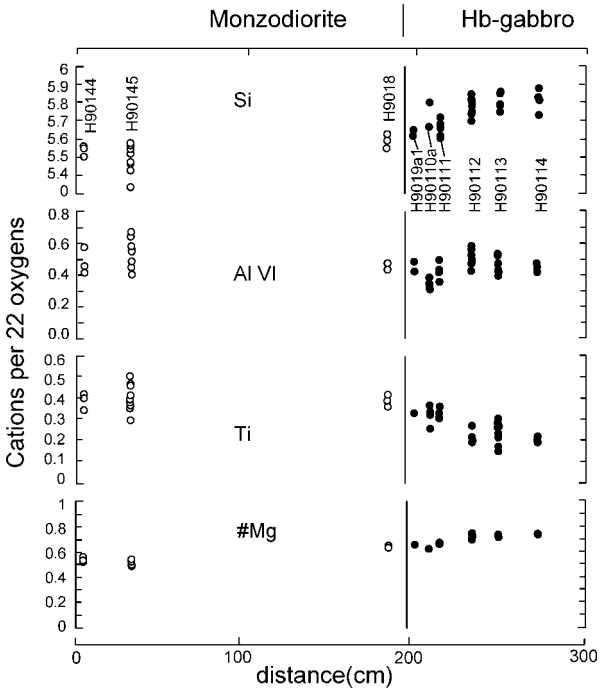

Fig. 8. Profile across the contact between Hb-gabbro and monzodiorite in the Garandones outcrop (see Fig. 7 for location of profile and sample locations), showing the variations in the composition of biotite.

euhedral plagioclase (0·3–1 cm) in the monzodiorite is indicative of crystallization from a water-rich magma or fluid. The contact relationships suggest that diorite segregated from the gabbroic magma leaving a hornblende-rich cumulate. This interpretation will be considered in a subsequent section based on geochemical variations across the interface separating the hornblende gabbro and monzodiorite. Apart from variations in the modal abundances of biotite and hornblende in the gabbro body towards the contact with the monzodiorite, there are interesting variations recorded in the chemical composition of the biotite. Table 1 shows representative mica analyses from the detailed profile indicated in Fig. 7. Figure 8 shows the main compositional variations in the chemistry of biotite across this profile. The Mg-number of biotite in the hornblende gabbro decreases slightly from 0·7 to 0·6 towards the interface and is somewhat lower ($\sim$0·5) in the monzodiorites. Most of these analyses are of biotites included within amphibole, a typical texture of appinitic hornblendites and hornblende gabbros. The most significant variation is displayed by Si and Ti. The good correlation between Si and Ti indicates that this variation is related to a Ti-Tschermak substitution, which is related to temperature variations: biotites richer in Ti equilibrated at higher temperatures compared with biotites poorer in Ti. The increase in Ti is towards the margin of the mafic body where the hornblende gabbro has a finer grain size, suggesting some chilling effect against the surrounding monzodiorite. This zoning is preserved from re-equilibration as a result of the coupling of Ti with tetrahedral Al in the biotite structure. Re-equilibration, however, may have affected the Mg-number of the biotite. The biotite compositional variations indicate that the margins of the mafic bodies crystallized earlier than the cores and that these margins recorded high-temperature conditions whereas re-equilibration by slow cooling dominated the cores. As noted above, the hornblende gabbro is never in direct contact with the migmatitic rocks, and is always separated from them by a zone of intermediate rocks of monzodiorite composition. The inference is that monzodiorites may therefore represent the by-products of some kind of reaction between fluids or melts extracted from the basic magmas and the anatectic rocks developed from the Ollo de Sapo gneisses. The intricacies of this reaction process can be better understood by examining the variation in major and trace element geochemistry across the hornblende–gabbro monzodiorite interface. These chemical variations for this particular outcrop and for the most representative rock types of the Sanabria complex are discussed in the next section.

WHOLE-ROCK COMPOSITIONS

Sampling and analytical techniques

To characterize the range of geochemical variation within the Sanabria complex, representative samples from each of the main rock types were analysed for major and trace elements. Selected samples from each group were also analysed for their Sr and Nd isotope composition. Apart from this general sampling, detailed sampling was carried out on the small-scale traverse across the contact between the hornblende gabbros and monzodiorites of the Garandones area, described above.

Major elements were analysed by X-ray fluorescence (XRF) at the University of Oviedo (Spain) using glass beads. The typical precision of the XRF technique was better than $\pm$1·5% relative. Trace elements and rare earth elements (REE) were analysed by inductively coupled plasma mass spectrometry (ICP-MS) with an HP-4500 system at the University of Huelva, following digestion in a HF + HNO_3 (8:3) solution, drying and second dissolution in 3 ml HNO_3 and later 3 ml HCl. The average precision and accuracy for most of the elements fall in the range of 5–10% relative, and they were controlled by repeated analysis of the SARM-1 (granite) and SARM-4 (norite) international rock standards. Rb–Sr and Sm–Nd isotopic ratios were

determined using a Finnigan MAT-262 mass spectrometer at the University of Granada and at the University of the Basque Country, Bilbao (Spain). Analytical details of the routine methods used at the University of Granada have been given by Montero & Bea (1998) and Bea *et al*. (1999). Two appinitic rocks (Table 3) were analysed in the Department of Geology of the University of the Basque Country. Sr and Rb and the REE were separated by specific extraction chromatography using the method described by Pin *et al*. (1994) and Pin & Santos Zalduegui (1996). The average $^{87}Sr/^{86}Sr$ for NBS987 during the analytical runs was 0·710245 ± 14. Nd isotopic ratios were corrected for mass fractionation using a $^{146}Nd/^{144}Nd$ ratio of 0·7219. During the course of this study the La Jolla Nd standard gave $^{143}Nd/^{144}Nd = 0·5118452 \pm 59$.

Representative results for major and trace elements analyses are given in Table 2. Table 3 reports the Sr and Nd isotopic data.

Major elements

The rocks of the Sanabria complex show a wide range in silica content from basaltic (gabbro) and ultramafic compositions to leucogranite. Monzodiorites, diorites and granodiorites are intermediate in composition. An important feature is the high content in K_2O even in the more basic compositions. The compositional trend displayed in the K_2O–silica diagram is of high-K to shoshonitic affinity (Fig. 9). Most hornblende gabbros have high MgO contents, normally >10 wt %. These samples correspond to blocks of several metres diameter that are enclosed by monzodiorites and diorites (e.g. the Garandones gabbros). In major element vs silica variation diagrams (Fig. 10) there appear to be two compositional trends, which converge at a silica value of ~63 wt %. These two trends are most distinct in the plot of Al_2O_3 vs SiO_2 and are therefore referred to as the high-Al and low-Al trends, respectively. The high-Al (HA) trend is defined by monzodiorites, Bt-diorites and Bt-tonalites. For MgO and Al_2O_3 this trend points towards the granodiorites and the Ollo de Sapo migmatites and related leucogranites. The low-Al (LA) trend is more curved for both Al_2O_3 and MgO and converges to the same silica-rich rocks (i.e. granodiorites and the Ollo de Sapo migmatites). For other major oxides such as Fe_2O_3 and CaO there is a single trend. The scattered distribution of alkalis Na_2O and K_2O makes it difficult to recognize these two trends. However, samples richer in alkalis are part of the HA trend in the low-silica region of the diagrams. Also depicted in these diagrams are the fields of hornblende gabbros and monzodiorites from the profile sampled in the Garandones Lake area. The arrows linking these fields indicate the enrichment in Al_2O_3 and alkalis and the depletion in Fe_2O_3, MgO and CaO in the monzodiorites with respect to the hornblende gabbros. It is important to note the distinct jump in composition between these two rock types, monzodiorites and hornblende gabbros. The observation that the monzodiorites of the Garandones profile are a part of the HA trend suggests that a detailed study of the local variations within this profile may help to understand the origin of these trends and hence the petrogenesis of an important part of the appinitic suite. The spatial variations across the contact between these two rock types are illustrated in Fig. 11 for selected major and trace elements. To avoid the constant sum effect, major element abundances have been normalized to 100 oxygens in these plots. The central part of the hornblende gabbro body is nearly homogeneous. Near the contact, a marked compositional gradient is observed for most major elements, with a distinct compositional jump across the contact. The profiles for Fe, Ti, K and Si are completely divergent at both sides of the contact. The meaning of these relations will be discussed below.

Trace elements and REE

Figure 12 shows chondrite-normalized REE patterns for representative samples from the Sanabria massif. The monzodiorites and banded diorites are enriched in light REE (LREE) (La/Yb > 300) with respect to the hornblende gabbros and granodiorites. The variability of the patterns suggests complex relationships between the gabbros, intermediate rocks and the granite–migmatite associations.

It is interesting to note the high content of Sr, Ba and LREE in most of the monzodiorites of the Sanabria complex (Table 2). Similar characteristics are found in Caledonian appinitic rocks (e.g. Rogart in Scotland, Fowler *et al*., 2001) and in other Variscan complexes (e.g. Guitiriz in Galicia, Menendez & Ortega, 1999; López Moro, 2000). Figure 13 shows silica variation diagrams for selected trace elements of petrogenetic interest. The two main trends, high-Al (HA) and low-Al (LA), identified from Fig. 10 are also recognized in the Cr and Ni variations. Hornblende gabbros and hornblende diorites form a continuous curvilinear trend converging with the HA trend in the field of the granodiorites. The point of convergence is around 63 wt % silica, such that intermediate rocks and granodiorites may be linked either to the LA trend with the hornblende gabbros or to the HA trend with the monzodiorites. Variations in Rb, Sr and Ba are not so clear in distinguishing the two evolutionary trends. Of particular interest is the correlation between LREE (e.g. La) and silica. Some monzodiorites show a vertical array with a strong enrichment in La up to 120 ppm with no

Table 2: Representative whole-rock analyses and mineral modes from the Sanabria complex

	Whole area													
	Hb gabbros and hornblendites				Monzodiorites				Hb diorites					
Locality:	Cárdenas	Cárdenas	Garandones	Garandones	Ribadelago	Garandones	Ribadelago	Ribadelago	Porto	Porto	Garandones	Ribadelago	Ribadelago	San Martín
Sample:	J5996	J5997	A59917	A59918	A119845	A59919	A119843	A119847	A119816	A59916	A59911	A119839	A119846	A109810
wt %														
SiO_2	48·28	48·83	51·48	53·04	52·60	52·73	53·38	54·61	55·05	56·14	58·01	59·78	61·18	61·63
TiO_2	0·58	1·28	0·66	0·83	1·09	1·25	1·57	0·81	0·76	0·71	0·65	0·68	0·63	0·66
Al_2O_3	9·28	14·10	15·20	15·01	21·25	20·14	20·18	20·88	16·41	15·85	15·66	15·41	16·49	16·56
Fe_2O_{3T}	9·83	8·71	7·46	8·39	5·95	6·89	7·36	5·04	6·62	6·91	6·60	5·73	5·33	4·89
MgO	18·88	12·61	10·56	8·64	3·83	4·31	2·71	3·29	7·57	7·35	6·53	6·82	4·10	3·35
MnO	0·14	0·11	0·12	0·14	0·07	0·07	0·09	0·06	0·10	0·10	0·11	0·11	0·08	0·07
CaO	7·68	8·70	7·74	7·35	5·65	5·75	5·04	5·13	6·41	5·59	3·30	4·74	5·28	4·35
Na_2O	1·05	2·09	1·47	2·49	4·05	3·28	3·68	3·75	2·58	2·61	1·53	2·44	3·20	3·29
K_2O	1·70	1·49	2·93	2·45	3·76	3·12	4·44	4·75	2·68	2·90	4·47	2·93	2·10	3·62
P_2O_5	0·11	0·10	0·19	0·31	0·53	0·47	0·47	0·54	0·16	0·16	0·48	0·15	0·17	0·23
LOI	2·61	2·04	2·33	1·20	1·21	1·35	0·82	1·19	1·54	1·31	2·04	1·16	0·89	0·79
Total	100·14	100·06	100·14	99·85	99·99	99·36	99·74	100·05	99·88	99·63	99·38	99·95	99·45	99·44
ppm														
Li	26·16	33·94	43·52	23·50	74·72	42·02	70·10	53·23	53·54	22·88	104·16	81·09	60·04	53·96
Be	1·01	1·16	1·79	1·95	3·15	2·54	2·58	2·34	2·06	2·52	3·49	1·91	5·10	4·44
Sc	23·06	30·34	22·92	25·21	6·92	10·60	9·96	5·03	16·51	17·17	15·59	15·32	15·48	10·44
V	104·72	217·46	131·59	122·58	118·04	110·30	104·20	96·75	93·57	133·50	71·49	95·29	82·32	80·84
Cr	1058·90	630·26	508·29	430·99	67·27	94·29	66·51	70·80	238·61	356·40	291·80	428·60	286·20	219·20
Co	45·95	41·32	31·86	28·68	15·65	19·16	13·03	12·66	25·51	27·50	20·30	21·45	14·30	15·36
Ni	259·50	180·63	167·41	147·59	11·61	28·18	5·57	11·02	108·58	136·80	131·64	127·20	57·19	44·86
Ga	19·65	29·04	54·61	42·51	75·72	74·97	90·04	109·80	34·09	51·09	40·63	43·20	36·55	63·11
Rb	49·09	44·99	124·68	78·90	149·55	123·47	160·50	125·90	83·61	107·60	209·42	135·20	97·20	170·60
Sr	208·55	459·00	597·17	578·90	626·68	769·29	587·30	574·70	532·62	535·50	278·12	399·80	472·40	570·90
Y	11·58	20·45	16·46	38·29	20·66	12·66	31·58	14·67	19·23	11·69	21·83	13·56	12·77	14·44
Zr	73·57	52·61	74·98	76·35	100·39	15·29	171·70	98·55	32·41	46·73	21·57	46·57	87·60	150·60
Nb	2·47	2·69	5·53	11·36	10·93	10·16	18·41	7·45	6·11	7·59	9·46	8·63	7·66	10·42
Cd	0·06	0·03	0·11	0·16	0·04	0·03	0·06	0·03	0·08	0·07	0·09	0·04	0·06	0·04
Cs	4·99	2·53	6·28	3·00	5·76	4·45	6·05	4·43	4·11	3·49	6·52	4·15	5·72	7·98
Ba	251·97	312·90	901·96	520·04	750·47	1208·72	1012·00	1425·00	333·49	753·60	470·22	358·90	269·50	955·90

Table 2: continued

	Whole area													
	Hb gabbros and hornblendites				Monzodiorites				Hb diorites					
Locality:	Cárdenas	Cárdenas	Garandones	Garandones	Ribadelago	Garandones	Ribadelago	Ribadelago	Porto	Porto	Garandones	Ribadelago	Ribadelago	San Martín
Sample:	J5996	J5997	A59917	A59918	A119845	A59919	A119843	A119847	A119816	A59916	A59911	A119839	A119846	A109810
La	13·49	14·53	39·47	35·96	78·28	57·84	96·39	112·80	21·29	24·25	19·36	22·99	17·30	40·73
Ce	30·48	36·09	74·89	106·41	168·31	116·66	219·30	238·00	49·08	56·37	44·45	48·12	47·30	88·39
Pr	3·83	5·16	9·59	15·15	18·32	12·44	24·30	25·17	6·70	6·23	5·82	6·16	4·81	9·34
Nd	15·75	22·81	36·94	69·74	64·97	43·96	88·70	85·16	27·72	23·36	24·59	24·11	18·43	33·34
Sm	3·12	5·23	6·19	16·03	11·12	6·85	16·01	12·46	5·90	4·24	5·58	5·11	4·01	6·11
Eu	0·82	1·34	1·52	2·18	2·10	1·90	2·26	2·11	1·35	1·14	1·04	1·05	1·12	1·34
Gd	2·82	4·89	4·81	13·05	8·47	5·17	12·07	8·36	4·87	3·43	5·07	4·28	3·40	4·65
Tb	0·40	0·79	0·61	1·71	1·00	0·58	1·45	0·85	0·67	0·44	0·79	0·60	0·48	0·59
Dy	2·38	4·12	3·29	8·82	4·86	2·92	6·98	3·68	3·78	2·44	4·63	3·17	2·66	3·11
Ho	0·46	0·77	0·61	1·54	0·85	0·48	1·23	0·61	0·72	0·44	0·86	0·56	0·50	0·55
Er	1·32	2·18	1·70	3·93	2·18	1·24	3·15	1·59	1·96	1·23	2·36	1·46	1·39	1·47
Tm	0·17	0·27	0·22	0·49	0·27	0·13	0·41	0·18	0·26	0·15	0·31	0·18	0·18	0·19
Yb	1·13	1·74	1·40	2·91	1·58	0·80	2·48	1·09	1·62	1·01	1·88	1·08	1·21	1·22
Lu	0·15	0·22	0·20	0·39	0·21	0·09	0·33	0·15	0·22	0·13	0·23	0·14	0·17	0·16
Pb	2·65	7·83	13·95	12·21	24·73	16·41	25·21	33·85	12·90	17·10	7·18	10·44	16·05	36·33
Th	5·71	4·56	10·83	5·51	30·53	16·00	29·32	44·17	6·57	12·74	3·98	6·60	12·05	19·96
U	1·23	1·16	2·27	1·59	3·57	1·25	5·04	3·53	0·83	1·20	1·75	1·06	0·48	5·56
Modal proportions (vol. %)														
Quartz	1·2	2·6	8·3	6·8	5·1	3·1	4·0	5·0	10·3	9·3	19·9	23·4	13·9	20·4
Plagioclase	2·2	18·6	36·5	38·3	63·1	56·1	68·5	67·3	45·7	44·2	32·5	35·9	46·8	47·5
K-feldspar	—	—	—	—	—	—	—	—	0·1	—	—	—	—	4·8
Biotite	33·4	19·4	16·9	21·2	30·7	40·1	25·5	27·4	25·4	33·5	47·1	29·7	28·2	22·3
Amphibole	62·0	57·9	38·1	33·0	—	—	—	—	18·5	13·0	—	10·8	11·0	4·5
Muscovite	—	—	—	—	—	—	—	—	—	—	—	—	—	—
Chlorite	0·6	—	0·1	—	—	—	—	—	—	—	0·1	—	0·1	—
Apatite	—	—	0·1	—	0·1	0·2	—	—	—	—	—	0·1	—	0·1
Opaques	0·6	1·4	—	—	0·1	0·5	0·7	—	—	—	0·1	—	—	0·1
Titanite	—	—	—	—	0·9	0·1	1·3	0·2	—	—	—	0·1	—	—
Zircon	—	0·1	—	—	—	—	—	0·1	—	—	—	—	—	0·3
Allanite	—	—	—	—	—	—	—	—	—	—	—	—	—	—
Epidote	—	—	—	—	—	—	—	—	—	—	—	—	—	—

	Whole area												
	Hb diorites	Bt diorites						Granodiorites					
Locality:	Ribadelago	Porto	Porto	Ribadelago	Porto	Garandones	Ribadelago	Cárdenas	Norte	Porto	Norte	Porto	Norte
Sample:	A119848	A119815	A119814	A119841	A119812	A59912	A11986	J5995	GC2559902	A11985	GC2559901	A119825	GC2559903
wt %													
SiO_2	62·38	57·09	58·00	58·07	59·94	60·64	61·3	61·72	63·33	63·41	66·88	66·9	67·61
TiO_2	0·68	0·92	1·09	1·19	0·92	0·75	0·81	0·93	0·73	1·01	0·56	0·57	0·50
Al_2O_3	15·19	18·56	18·31	19·02	17·87	17·7	17·55	17·25	16·95	17·45	15·92	16·31	15·54
Fe_2O_{3T}	5·78	6·50	6·42	6·43	6·20	5·44	5·38	5·20	4·49	4·83	3·36	3·54	3·11
MgO	4·95	3·94	3·93	2·34	2·77	2·23	2·28	2·83	2·13	1·40	1·38	1·38	1·50
MnO	0·08	0·08	0·08	0·07	0·11	0·07	0·06	0·07	0·06	0·04	0·04	0·04	0·04
CaO	3·73	5·17	4·82	5·18	5·20	4·05	4·08	3·99	2·95	2·85	2·08	2·13	2·79
Na_2O	2·59	3·20	3·12	3·63	2·73	3·73	3·70	3·24	3·47	3·65	3·13	3·15	3·66
K_2O	2·97	2·84	3·11	3·09	2·49	3·23	3·31	3·10	3·72	3·91	4·65	4·82	3·59
P_2O_5	0·13	0·23	0·30	0·31	0·28	0·40	0·31	0·19	0·30	0·32	0·27	0·26	0·25
LOI	1·48	1·10	0·90	0·78	1·26	0·84	0·81	0·85	1·13	1·18	0·96	0·98	0·87
Total	99·96	99·63	100·08	100·11	99·77	99·08	99·59	99·37	99·26	100·05	99·23	100·08	99·46
ppm													
Li	93·91	38·86	42·13	79·28	84·72	40·19	51·97	38·01	81·02	67·48	60·45	54·92	61·22
Be	2·98	2·42	2·27	2·59	3·17	3·55	3·39	3·94	6·10	2·74	3·78	3·25	4·06
Sc	16·66	12·15	12·01	8·32	13·91	5·89	6·42	9·92	7·09	2·98	5·82	5·53	7·46
V	77·08	119·50	129·94	99·19	127·20	74·79	75·47	96·00	57·00	46·02	39·57	38·20	50·03
Cr	396·70	192·50	166·93	97·39	121·60	62·01	186·30	98·10	122·90	91·08	82·12	170·00	74·54
Co	18·13	16·93	17·56	11·06	11·75	10·01	11·61	12·46	8·76	7·23	5·95	5·77	5·11
Ni	109·00	20·72	22·00	5·74	4·72	18·18	20·34	16·59	13·95	3·62	12·14	7·71	6·42
Ga	39·72	52·73	55·25	94·71	71·17	85·72	72·14	50·59	50·44	76·43	57·12	74·57	62·13
Rb	152·50	113·80	144·08	132·46	97·46	122·60	154·10	137·80	205·89	130·04	196·10	192·90	122·40
Sr	370·70	493·30	456·71	701·16	750·80	1015·00	755·70	404·40	372·19	536·44	322·20	327·60	791·50
Y	8·96	12·54	9·43	25·13	28·57	10·66	7·59	9·52	16·26	6·98	14·53	13·39	15·35
Zr	38·19	23·47	7·54	122·65	69·53	188·80	55·90	35·30	72·86	155·08	116·30	110·10	154·60
Nb	12·56	9·01	8·13	18·88	11·76	10·55	10·42	10·34	10·80	13·35	7·95	7·65	7·35
Cd	0·05	0·05	0·03	0·04	0·12	0·08	0·04	0·04	0·07	0·27	0·13	0·08	0·06
Cs	9·13	5·07	5·28	12·51	6·72	4·40	4·33	5·83	11·00	4·92	8·19	7·60	4·23
Ba	313·00	701·70	701·53	1086·56	1089·00	1447·00	1020·00	694·40	585·35	1108·22	767·90	773·90	894·20
La	12·40	28·17	19·63	48·89	43·24	112·00	66·64	40·76	37·70	51·14	42·78	40·80	46·92
Ce	39·94	51·80	39·64	96·54	98·49	210·70	117·00	89·82	82·50	108·50	92·96	84·02	98·51

Table 2: continued

	Whole area												
	Hb diorites	Bt diorites						Granodiorites					
Locality:	Ribadelago	Porto	Porto	Ribadelago	Porto	Garandones	Ribadelago	Cárdenas	Norte	Porto	Norte	Porto	Norte
Sample:	A119848	A119815	A119814	A119841	A119812	A59912	A11986	J5995	GC2559902	A11985	GC2559901	A119825	GC2559903
Pr	3·17	6·33	4·84	12·36	10·65	21·72	12·62	9·39	8·94	11·47	10·24	9·72	11·07
Nd	12·44	23·45	18·45	48·86	39·08	72·98	43·25	32·85	31·59	40·84	36·46	35·10	40·19
Sm	2·94	4·33	3·49	10·22	7·20	9·77	6·20	5·55	5·58	6·72	6·84	6·58	7·19
Eu	0·87	1·41	1·43	2·16	1·86	2·06	1·55	1·46	1·18	1·61	1·32	1·36	1·66
Gd	2·68	3·54	2·72	8·61	6·10	5·97	4·17	3·98	4·44	4·54	5·25	5·15	5·09
Tb	0·36	0·47	0·35	1·15	0·88	0·60	0·43	0·47	0·61	0·44	0·67	0·64	0·60
Dy	2·10	2·58	1·90	5·86	5·37	2·63	1·89	2·30	3·35	1·75	3·22	3·12	3·08
Ho	0·37	0·48	0·34	1·01	1·09	0·39	0·29	0·37	0·58	0·23	0·53	0·52	0·54
Er	0·96	1·27	0·87	2·50	3·11	0·99	0·68	0·94	1·57	0·52	1·40	1·37	1·53
Tm	0·12	0·16	0·11	0·30	0·44	0·10	0·07	0·09	0·19	0·05	0·18	0·17	0·19
Yb	0·76	1·00	0·57	1·74	2·85	0·66	0·45	0·63	1·24	0·31	1·08	1·08	1·30
Lu	0·10	0·13	0·07	0·21	0·40	0·08	0·05	0·07	0·15	0·03	0·15	0·14	0·17
Pb	12·32	17·03	16·35	20·15	16·33	34·37	27·40	20·00	26·87	27·67	35·70	36·49	35·97
Th	6·81	9·56	4·96	18·47	14·82	41·63	23·94	16·71	12·02	16·15	21·16	21·08	18·80
U	8·06	1·69	0·95	3·49	5·93	5·09	2·68	2·05	3·75	2·37	3·25	3·19	6·33
Modal proportions (vol. %)													
Quartz	23·2	14·3	14·6	12·9	31·1	14·9	19·1	16·8	25·1	22·6	18·2	31·1	27·4
Plagioclase	41·4	51·1	48·7	51·5	48·5	56·8	42·4	49·6	47·3	45·2	40·7	31·5	33·2
K-feldspar	—	0·3	—	2·6	3·2	1·2	16·4	4·6	6·2	10·1	22·9	18·0	12·2
Biotite	29·1	33·0	36·1	30·3	17·1	26·3	21·6	27·7	18·6	16·0	13·8	13·3	20·7
Amphibole	6·2	0·9	—	—	—	—	—	—	—	—	—	—	—
Muscovite	—	—	—	—	—	—	—	0·9	2·5	3·2	5·4	5·7	6·0
Chlorite	—	—	—	—	—	—	—	—	0·2	2·2	—	0·2	0·1
Apatite	—	0·1	0·3	0·3	—	—	—	0·4	0·1	—	—	0·2	0·2
Opaques	0·1	—	0·1	0·1	—	—	—	—	—	0·7	—	—	0·2
Titanite	—	—	0·1	2·3	—	0·1	0·5	—	—	—	—	—	—
Zircon	—	0·1	0·1	—	0·1	—	—	—	—	—	—	—	—
Allanite	—	—	—	—	—	0·7	—	—	—	—	—	—	—
Epidote	—	—	—	—	—	—	—	—	—	—	—	—	—

	Whole area											
	Leucogranites				Migmatite leucosomes		Migmatites					
Locality:	P. Blancas	Porto	Manca	Campo 2nd.	Playa	Playa	Ribadelago	Ribadelago	Ribadelago	Ribadelago	Ribadelago	Garandones
Sample:	A11984	A11987	A59931	GC2559905	GC2859901L2	GC2859904L	A119826	A119827	A119829	A119830	A119833	A59921
wt %												
SiO_2	72·12	72·51	70·64	72·51	74·17	73·55	65·32	63·22	65·57	66·31	68·8	67·69
TiO_2	0·23	0·23	0·17	0·20	0·07	0·08	0·52	0·55	0·55	0·55	0·47	0·56
Al_2O_3	14·93	14·75	15·65	14·53	14·53	14·69	16·20	17·02	16·56	16·85	15·47	15·58
Fe_2O_{3T}	1·69	1·60	1·33	1·44	0·66	0·66	4·84	5·28	5·10	4·42	4·33	4·09
MgO	0·42	0·45	0·37	0·42	0·22	0·23	2·09	2·32	2·13	1·86	1·71	1·53
MnO	0·02	0·02	0·03	0·02	0·01	0·01	0·06	0·06	0·06	0·03	0·04	0·04
CaO	0·88	1·05	0·96	0·77	1·19	0·97	0·90	0·74	1·48	1·02	1·26	1·67
Na_2O	3·41	3·36	4·11	3·25	3·43	3·36	2·73	2·61	2·42	2·39	2·69	3·15
K_2O	4·94	4·95	4·96	4·84	4·33	5·00	4·45	4·71	3·67	4·56	3·74	3·77
P_2O_5	0·30	0·11	0·15	0·29	0·07	0·07	0·16	0·17	0·15	0·17	0·17	0·17
LOI	0·85	0·74	0·79	1·06	0·62	0·66	2·63	3·01	2·20	1·77	1·50	0·94
Total	99·79	99·77	99·16	99·33	99·30	99·28	99·90	99·69	99·89	99·93	100·18	99·19
ppm												
Li	77·06	37·60	47·20	49·56	10·75	7·79	43·63	54·04	53·92	53·77	47·43	56·46
Be	4·81	3·52	5·39	4·69	1·98	1·69	2·53	3·10	3·73	2·49	3·21	2·69
Sc	2·37	2·99	2·52	2·34	1·17	1·28	7·52	9·74	9·25	8·84	7·94	9·26
V	10·99	10·81	9·76	9·91	7·40	6·35	45·51	61·00	56·06	57·15	47·88	56·79
Cr	205·53	224·55	147·60	129·80	162·23	147·84	168·53	272·41	249·60	203·20	245·10	117·50
Co	1·94	2·16	1·85	1·53	1·18	1·03	6·99	8·92	9·25	7·91	9·88	7·78
Ni	4·87	4·76	10·55	16·94	6·87	3·43	15·16	20·36	19·81	18·92	17·88	19·90
Ga	39·25	44·98	41·99	41·20	66·89	84·58	60·42	78·63	63·86	77·42	63·12	50·20
Rb	227·09	132·75	197·40	232·50	80·57	96·10	148·52	177·14	119·90	142·30	126·60	135·30
Sr	157·62	164·00	162·10	161·30	285·58	319·22	128·98	147·50	178·70	151·30	140·30	178·90
Y	7·14	6·52	8·20	7·40	4·32	2·08	15·36	16·80	12·32	13·65	13·79	14·21
Zr	70·76	104·71	60·97	74·47	22·31	36·96	14·59	16·81	13·01	22·66	18·69	25·72
Nb	8·37	4·77	7·75	9·23	1·55	1·56	8·55	10·03	9·52	9·74	8·67	12·21
Cd	0·05	0·06	0·07	0·05	0·04	0·04	0·05	0·07	0·09	0·05	0·08	0·09
Cs	7·18	6·73	5·48	7·41	1·75	2·55	4·66	5·22	5·23	8·35	5·58	5·09
Ba	330·67	525·52	468·90	383·40	1091·69	1418·88	667·67	826·28	638·50	782·30	583·30	605·80
La	21·33	25·19	28·21	21·89	7·17	5·51	27·85	30·94	31·35	33·17	29·61	30·44
Ce	44·10	50·54	52·44	44·23	13·74	10·63	58·18	63·89	65·46	71·12	61·04	63·72

Table 2: continued

	Whole area											
	Leucogranites				Migmatite leucosomes		Migmatites					
Locality:	P. Blancas	Porto	Manca	Campo 2nd.	Playa	Playa	Ribadelago	Ribadelago	Ribadelago	Ribadelago	Ribadelago	Garandones
Sample:	A11984	A11987	A59931	GC2559905	GC2859901L2	GC2859904L	A119826	A119827	A119829	A119830	A119833	A59921
Pr	5·13	5·82	5·95	5·22	1·66	1·26	7·00	7·79	7·80	8·55	7·48	7·76
Nd	18·10	20·75	21·20	18·80	6·26	4·67	26·51	29·03	29·50	32·51	28·43	29·71
Sm	3·62	4·24	3·57	3·77	1·32	0·93	5·46	5·73	5·96	6·74	5·84	6·15
Eu	0·58	0·92	0·95	0·65	0·98	0·97	1·30	1·37	1·41	1·53	1·29	1·28
Gd	2·70	3·15	2·68	2·85	1·12	0·75	4·78	4·97	4·98	5·77	5·01	5·21
Tb	0·33	0·37	0·33	0·36	0·14	0·08	0·69	0·70	0·66	0·77	0·68	0·68
Dy	1·56	1·66	1·71	1·66	0·84	0·43	3·78	3·86	3·24	3·66	3·43	3·44
Ho	0·23	0·25	0·26	0·23	0·13	0·06	0·68	0·72	0·53	0·59	0·58	0·54
Er	0·56	0·57	0·70	0·62	0·40	0·18	1·84	1·93	1·23	1·35	1·43	1·31
Tm	0·07	0·06	0·08	0·07	0·04	0·01	0·24	0·26	0·14	0·15	0·17	0·14
Yb	0·47	0·45	0·58	0·52	0·34	0·17	1·49	1·62	0·81	0·89	1·02	0·88
Lu	0·05	0·06	0·07	0·06	0·03	0·01	0·20	0·22	0·10	0·11	0·13	0·10
Pb	29·67	44·23	46·22	33·18	37·88	35·55	25·53	26·06	23·53	21·78	18·29	30·76
Th	9·63	16·02	11·49	9·63	2·20	1·57	12·60	13·23	11·92	13·27	12·07	12·05
U	4·29	5·15	3·96	5·30	1·27	0·85	2·63	2·92	2·61	2·97	3·39	3·94
Modal proportions (vol. %)												
Quartz	40·4	35·1	34·2	38·3	45·4	44·4	31·1	22·0	39·8	39·7	46·1	42·1
Plagioclase	29·3	40·3	34·6	33·2	23·2	25·2	41·7	35·2	21·3	11·6	20·4	23·4
K-feldspar	16·9	13·5	23·8	18·9	22·0	21·6	6·8	16·4	7·4	4·6	2·1	13·0
Biotite	5·4	6·4	3·5	5·3	0·6	0·1	—	—	20·6	18·9	16·4	13·7
Amphibole	—	—	—	—	—	—	—	—	—	—	—	—
Muscovite	7·4	4·7	3·7	4·0	7·5	8·0	4·6	6·3	6·4	24·9	14·9	5·7
Chlorite	0·2	—	—	—	1·3	0·7	15·3	19·0	4·4	0·3	—	2·1
Apatite	0·4	—	0·2	0·3	—	—	—	—	0·1	—	—	—
Opaques	—	—	—	—	—	—	0·7	1·1	—	—	—	—
Titanite	—	—	—	—	—	—	—	—	—	—	—	—
Zircon	—	—	—	—	—	—	—	—	—	—	—	—
Allanite	—	—	—	—	—	—	—	—	—	—	—	—
Epidote	—	—	—	—	—	—	—	—	—	—	—	—

	Whole area										
	Migmatites	Augen-gneiss									
Locality:	Ribadelago	S Martín	S Martín	S Martín	S Martín	S Martín	Ribadelago	Vega Conde	Vega Conde	Vega Conde	Vega Conde
Sample:	A119835	A10985	A10989	A109811	A10986	A109812	A119834	A119824	A119821	A119817	A119823
wt %											
SiO_2	70·54	64·56	65·93	66·19	66·41	66·44	68·36	67·09	67·56	67·96	70·33
TiO_2	0·48	0·70	0·77	0·63	0·53	0·73	0·51	0·60	0·59	0·52	0·47
Al_2O_3	14·5	17·00	16·11	16·23	16·46	16·3	15·14	15·79	15·75	15·69	14·51
Fe_2O_{3T}	4·61	4·58	5·52	4·65	4·61	5·08	4·36	4·60	4·56	3·69	4·01
MgO	1·73	1·96	1·91	1·64	1·83	1·80	1·54	1·60	1·65	1·47	1·38
MnO	0·05	0·05	0·07	0·04	0·05	0·05	0·04	0·04	0·05	0·03	0·04
CaO	1·12	3·14	1·52	0·69	1·54	1·27	1·00	1·27	0·58	1·19	0·80
Na_2O	1·99	3·55	3·07	1·92	2·42	2·85	2·10	2·65	2·43	3·58	2·90
K_2O	3·56	3·01	3·46	4·62	3·94	3·90	4·77	4·00	4·05	3·94	4·14
P_2O_5	0·20	0·25	0·20	0·15	0·18	0·20	0·18	0·21	0·21	0·21	0·17
LOI	1·35	1·26	1·43	2·80	1·57	1·38	1·39	1·60	2·31	1·39	1·18
Total	100·13	100·06	99·99	99·56	99·54	100	99·39	99·45	99·74	99·67	99·93
ppm											
Li	46·71	59·64	41·20	38·34	58·07	51·11	56·17	51·47	40·11	38·56	36·11
Be	2·81	1·40	2·66	2·45	2·65	2·46	1·69	1·95	2·35	2·14	1·70
Sc	7·86	9·72	13·55	10·90	8·30	12·27	8·16	9·48	9·45	8·54	8·02
V	45·28	60·15	88·12	71·03	54·55	85·53	53·12	60·37	57·92	51·83	51·29
Cr	273·30	168·64	184·90	205·70	182·60	188·30	232·45	142·80	84·57	174·90	184·90
Co	8·05	8·63	11·99	9·80	8·24	6·95	8·00	4·90	8·17	7·20	6·65
Ni	18·81	10·51	28·30	19·53	18·38	14·88	21·63	10·42	18·48	18·06	15·05
Ga	57·88	44·36	54·91	59·49	52·96	55·27	58·22	65·69	46·52	47·12	68·30
Rb	127·00	127·25	133·20	186·60	157·10	155·20	157·91	135·80	134·00	130·50	152·10
Sr	86·20	331·07	176·60	102·70	156·20	140·60	117·90	138·60	68·95	130·80	78·26
Y	13·24	15·84	35·37	18·05	16·60	21·82	14·39	19·73	25·02	27·39	19·04
Zr	18·76	79·14	46·35	29·58	17·05	33·46	26·36	38·39	29·77	32·98	27·54
Nb	9·30	10·98	14·49	12·94	10·50	13·38	10·41	11·00	10·88	10·30	8·99
Cd	0·04	0·08	0·13	0·02	0·13	0·06	0·06	0·04	n.d.	0·07	0·05
Cs	7·36	4·45	7·14	7·09	4·86	6·52	6·90	3·89	5·05	4·59	4·24
Ba	500·20	538·60	768·90	838·10	717·10	731·30	509·70	679·70	516·60	505·20	721·70
La	28·85	44·58	44·42	41·56	30·66	40·46	31·91	27·23	28·46	28·55	25·03
Ce	61·10	98·04	100·70	91·44	72·27	95·62	67·80	58·37	60·81	59·82	57·61

Table 2: continued

	Whole area										
	Migmatites	Augen-gneiss									
Locality:	Ribadelago	S Martín	S Martín	S Martín	S Martín	S Martín	Ribadelago	Vega Conde	Vega Conde	Vega Conde	Vega Conde
Sample:	A119835	A10985	A10989	A109811	A10986	A109812	A119834	A119824	A119821	A119817	A119823
Pr	7·33	10·43	11·25	10·46	7·91	10·35	8·16	7·05	7·66	7·42	6·55
Nd	28·15	37·45	42·39	39·43	29·29	38·62	30·82	26·84	28·96	27·83	24·87
Sm	5·87	6·74	8·88	8·20	6·00	8·09	6·41	5·70	6·15	6·03	5·24
Eu	1·14	1·48	1·54	1·45	1·16	1·38	1·12	1·10	1·00	1·11	1·00
Gd	5·05	5·13	8·00	6·87	5·25	6·99	5·45	5·05	5·37	5·63	4·71
Tb	0·69	0·68	1·20	0·92	0·72	0·94	0·74	0·75	0·82	0·86	0·70
Dy	3·44	3·61	6·89	4·59	3·83	4·94	3·73	4·31	4·91	5·07	4·17
Ho	0·56	0·63	1·34	0·74	0·64	0·87	0·61	0·81	0·97	1·00	0·78
Er	1·35	1·66	3·72	1·72	1·62	2·21	1·47	2·19	2·69	2·78	2·12
Tm	0·15	0·21	0·48	0·19	0·19	0·27	0·17	0·29	0·38	0·38	0·28
Yb	0·91	1·26	3·02	1·12	1·14	1·67	0·99	1·83	2·26	2·29	1·72
Lu	0·11	0·17	0·40	0·14	0·14	0·22	0·13	0·25	0·31	0·31	0·23
Pb	17·08	23·44	22·01	27·28	36·73	22·35	28·07	20·63	54·29	26·85	18·66
Th	11·78	20·22	16·13	15·21	12·89	14·71	12·93	13·47	12·57	11·54	10·47
U	3·23	3·00	3·52	4·48	3·00	3·42	4·94	3·28	2·75	3·66	2·38
Modal proportions (vol. %)											
Quartz	41·6	35·4	30·7	32·5	29·2	21·8	34·4	50·7	45·4	36·2	38·0
Plagioclase	21·5	23·9	16·2	0·8	45·1	3·6	1·9	14·5	—	1·1	3·0
K-feldspar	1·5	11·7	—	19·1	1·1	13·2	27·2	5·4	9·0	18·4	17·6
Biotite	19·4	19·5	26·2	25·6	17·7	31·3	18·4	17·9	—	18·7	20·3
Amphibole	—	—	—	—	—	—	—	—	—	—	—
Muscovite	15·0	5·5	19·1	14·9	1·4	7·2	10·8	10·2	9·0	16·5	13·7
Chlorite	1·0	3·8	7·3	7·0	5·4	21·4	7·1	1·1	36·3	9·0	7·3
Apatite	—	—	—	—	0·1	—	0·1	0·1	—	—	—
Opaques	—	0·2	0·5	0·1	—	0·7	0·1	0·1	—	0·1	0·1
Titanite	—	—	—	—	—	—	—	—	—	—	—
Zircon	—	—	—	—	—	—	—	—	—	—	—
Allanite	—	—	—	—	—	—	—	—	—	—	—
Epidote	—	—	—	—	—	0·7	—	—	—	—	—

	Garandones profile (Fig. 6)									
	Gabbros						Monzodiorites			
Locality:	Garandones	Garandones	Garandones	Garandones	Garandones	Garandones	Garandones	Garandones	Garandones	Garandones
Sample:	H9019a1	H90110a	H90111	H90112	H90113	H90114	H90144	H90145	H9018	H9019a2
wt %										
SiO_2	44·17	44·95	47·88	51·00	51·62	51·86	55·66	48·69	54·22	55·23
TiO_2	2·08	1·86	1·30	0·70	0·66	0·65	1·20	1·47	1·26	0·92
Al_2O_3	12·86	12·49	10·82	11·26	11·10	11·39	20·20	21·87	19·75	21·12
Fe_2O_{3T}	12·61	12·59	11·80	9·24	8·80	8·36	5·77	7·39	5·70	4·27
MgO	13·07	13·55	14·01	14·02	14·50	14·30	3·27	3·99	4·53	3·42
MnO	0·17	0·16	0·17	0·15	0·14	0·13	0·05	0·07	0·05	0·04
CaO	8·25	8·03	8·33	7·38	7·45	7·31	5·43	6·11	5·88	6·63
Na_2O	1·00	0·98	0·99	1·37	1·40	1·56	4·02	4·09	3·03	3·37
K_2O	3·35	3·20	2·54	2·49	2·21	2·21	2·71	3·44	3·33	2·61
P_2O_5	0·13	0·13	0·19	0·19	0·18	0·18	0·27	1·12	0·61	0·18
LOI	2·02	1·72	1·96	1·92	1·90	1·81	0·92	0·97	1·14	1·95
Total	99·71	99·66	99·99	99·72	99·96	99·76	99·5	99·21	99·50	99·74
ppm										
Li	45·88	47·95	40·02	33·09	31·52	31·53	55·09	58·76	42·94	29·94
Be	1·68	1·62	1·50	1·28	1·23	1·39	3·91	3·16	2·47	2·48
Sc	42·96	42·21	37·27	29·72	28·88	29·05	20·19	15·41	11·13	9·38
V	284·66	253·33	151·51	126·02	127·02	129·76	129·37	125·83	117·77	97·17
Cr	788·26	777·40	862·78	935·92	908·91	905·13	166·51	67·19	125·90	192·88
Co	46·07	46·81	42·32	45·64	44·40	44·51	19·04	21·57	20·92	18·01
Ni	189·53	226·18	213·75	279·72	256·21	273·66	20·67	6·91	27·11	48·72
Ga	70·42	62·92	42·42	43·90	47·94	48·13	88·38	84·37	102·57	76·24
Rb	101·27	96·29	73·93	70·68	66·39	68·40	109·51	145·28	114·55	94·35
Sr	225·63	235·10	239·53	426·21	403·05	426·43	721·96	707·11	961·98	1142·08
Y	37·31	35·78	34·45	17·46	14·37	14·98	12·24	34·52	12·19	7·88
Zr	96·78	108·29	131·43	105·16	102·58	107·43	75·92	47·13	54·93	56·08
Nb	11·23	10·83	9·95	5·07	4·43	4·61	7·37	13·04	7·32	5·72
Cd	0·13	0·17	0·16	0·15	0·13	0·17	0·04	0·05	0·05	0·05
Cs	5·89	5·00	4·23	4·52	4·04	4·61	4·29	7·81	5·52	5·08
Ba	1296·17	1106·22	497·25	561·90	608·02	612·39	1210·38	1289·60	1910·51	1264·91
La	36·11	43·08	44·12	39·70	36·88	37·80	46·16	57·45	43·76	43·85
Ce	137·20	141·72	144·36	75·70	67·87	70·51	74·47	106·39	70·18	69·72

Table 2: continued

	Garandones profile (Fig. 6)									
	Gabbros						Monzodiorites			
Locality:	Garandones	Garandones	Garandones	Garandones	Garandones	Garandones	Garandones	Garandones	Garandones	Garandones
Sample:	H9019a1	H90110a	H90111	H90112	H90113	H90114	H90144	H90145	H9018	H9019a2
Pr	17·49	17·71	17·65	11·09	9·45	10·02	10·07	16·33	9·89	9·07
Nd	77·98	75·32	73·95	42·72	35·61	37·97	36·34	65·61	36·42	30·88
Sm	16·04	15·42	14·63	7·09	5·91	6·13	5·54	12·66	5·69	4·19
Eu	3·68	3·09	2·79	1·72	1·50	1·56	1·79	2·27	1·77	1·73
Gd	12·91	12·09	11·65	5·61	4·58	4·75	4·34	10·85	4·74	3·27
Tb	1·73	1·63	1·54	0·73	0·59	0·62	0·47	1·47	0·56	0·37
Dy	8·97	8·54	8·22	3·85	3·12	3·25	2·54	7·78	2·64	1·70
Ho	1·72	1·62	1·56	0·75	0·62	0·64	0·42	1·33	0·49	0·33
Er	4·40	4·14	4·08	1·99	1·66	1·72	1·06	3·19	1·22	0·80
Tm	0·59	0·56	0·57	0·29	0·25	0·25	0·10	0·35	0·17	0·13
Yb	3·25	3·10	3·25	1·74	1·44	1·48	0·73	2·05	0·87	0·59
Lu	0·46	0·45	0·47	0·26	0·22	0·22	0·06	0·24	0·12	0·09
Pb	12·49	10·90	23·59	19·71	20·24	20·46	20·71	26·29	21·10	19·75
Th	3·59	4·55	8·03	8·05	9·20	8·90	10·24	12·26	8·09	9·55
U	6·75	4·34	3·75	1·82	1·71	3·18	1·47	2·20	2·78	2·25
Modal proportions (vol. %)										
Quartz	2·1	2·1	3·8	4·2	5·4	7·5	14·1	5·2	21·7	9·5
Plagioclase	6·5	15·1	7·3	8·3	8·7	13·5	56·1	62·6	50·3	62·9
K-feldspar	—	—	—	—	—	—	—	—	—	—
Biotite	51·7	44·5	37·5	35·8	33·1	21·7	29·3	30·5	26·2	26·2
Amphibole	36·8	34·5	49·8	50·8	51·8	56·9	—	—	—	—
Muscovite	—	—	—	—	0·1	—	—	—	—	0·3
Chlorite	—	—	—	—	0·1	—	—	0·2	—	0·2
Apatite	0·1	—	—	—	—	—	0·5	1·5	1·0	0·1
Opaques	1·0	0·3	1·0	0·6	0·7	0·4	—	—	—	0·3
Titanite	1·4	3·2	0·6	0·3	—	—	—	—	0·1	0·5
Zircon	—	—	—	—	0·1	—	—	—	0·1	—
Allanite	—	—	—	—	—	—	—	—	0·3	—
Epidote	—	—	—	—	—	—	—	—	—	—

n.d., not detected.

Table 3: Isotope analyses of representative rocks from the Sanabria complex

Sample	Rock type	Rb (ppm)	Sr (ppm)	$^{87}Rb/^{86}Sr$	$^{87}Sr/^{86}Sr$	$\pm2\sigma$	$^{87}Sr/^{86}Sr_{t=345}$	Sm (ppm)	Nd (ppm)	$^{147}Sm/^{144}Nd$	$^{143}Nd/^{144}Nd$	$\pm2\sigma$	$^{143}Nd/^{144}Nd_{t=345}$	$\varepsilon_{Nd\ t=345}$	T_{DM}
J5996*	Hornblendite							3·24	15·95	0·1228	0·512467	8	0·512190	−0·1	1·06
J5997	Hb-gabbro	45·33	429·44	0·3054	0·70654	3	0·705040	5·27	23·81	0·1338	0·512460	7	0·512158	−0·7	1·11
A59917*	Hb-gabbro							6·04	37·48	0·0975	0·512305	8	0·512085	−2·1	1·22
A59918	Hb-gabbro	80·26	554·72	0·4186	0·70822	2	0·706166	15·93	69·98	0·1376	0·512297	9	0·511986	−4·1	1·37
A59919	Monzodiorite	123·68	689·02	0·5194	0·70878	2	0·706231	6·4	40·22	0·0962	0·512231	15	0·512014	−3·5	1·33
A59910B	Banded diorite	163	505·41	0·9333	0·71025	2	0·705670	6·29	30·94	0·1229	0·512281	8	0·512003	−3·7	1·35
J5995	Bt-diorite	134·8	418	0·9332	0·71152	2	0·706936	5·38	32·46	0·1002	0·512161	10	0·511935	−5·1	1·45
GC2559901	Granodiorite	210·4	329·55	1·8489	0·71703	2	0·707953	6·77	37·89	0·1081	0·512204	10	0·511960	−4·6	1·41
A11984	Leucogranite	231·01	156·93	4·2669	0·72675	3	0·705794	3·56	17·87	0·1204	0·512174	9	0·511902	−5·7	1·50
GC2859901L2	Migmatite leucosome	96·36	292·76	0·9528	0·71326	2	0·708576	1·18	5·41	0·1315	0·512213	15	0·511916	−5·4	1·48
A59921	Migmatite	143·43	168·6	2·4656	0·72528	2	0·713169	6·4	31·38	0·1234	0·512173	7	0·511894	−5·8	1·51
A109811	Ollo de Sapo gneiss	207·44	118·05	5·0988	0·73762	2	0·712583	8·48	41·78	0·1228	0·512185	8	0·511908	−5·6	1·49

CHUR values: $^{87}Rb/^{86}Sr = 0·0847$, $^{87}Sr/^{86}Sr = 0·7047$, $^{147}Sm/^{143}Nd = 0·1967$, $^{143}Nd/^{144}Nd = 0·512638$.
2σ: standard deviation.
*Samples analysed at the University of the Basque Country.

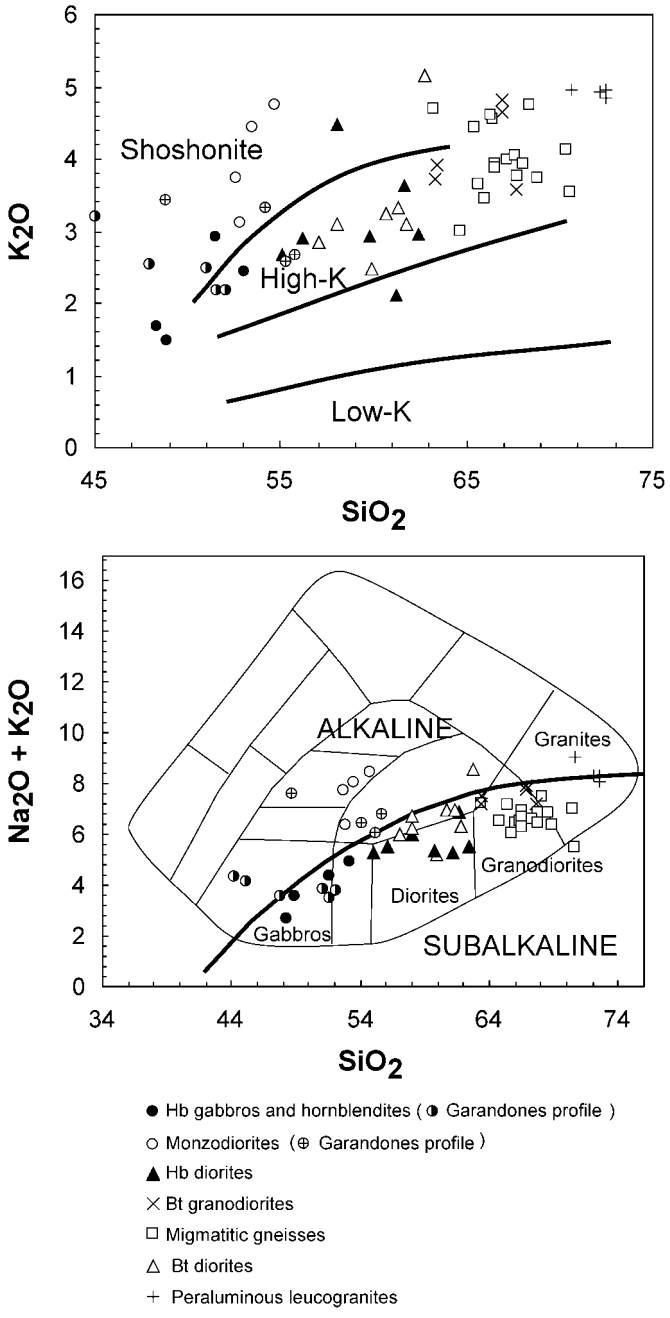

Fig. 9. Harker variation diagrams showing the range of geochemical variation in the Sanabria complex. Gabbros and monzodiorites plot in the field of high-K to shoshonitic series (a). With the exception of the monzodiorites, all the samples define a coherent trend in the total alkalis vs silica (TAS) diagram (b) from gabbro to granite. The series divisions in the K_2O–silica diagram (a) are from Le Maitre *et al.* (1989). Field divisions in the TAS diagram according to Le Maitre *et al.* (1989).

enrichment in silica, orthogonal to the main trend defined by the gabbros and the remaining intermediate rocks, granodiorites and migmatites. With regard to the relations between the hornblende gabbros and the monzodiorites of the Garandones profile, enrichments and depletions similar to those found in major element variations are observed. The monzodiorites are depleted in Cr and Ni and enriched in Rb, Sr and REE with respect to the hornblende gabbros.

Sr and Nd isotopic ratios

Sr and Nd isotopic ratios have been analysed for representative samples from the Sanabria complex; the data

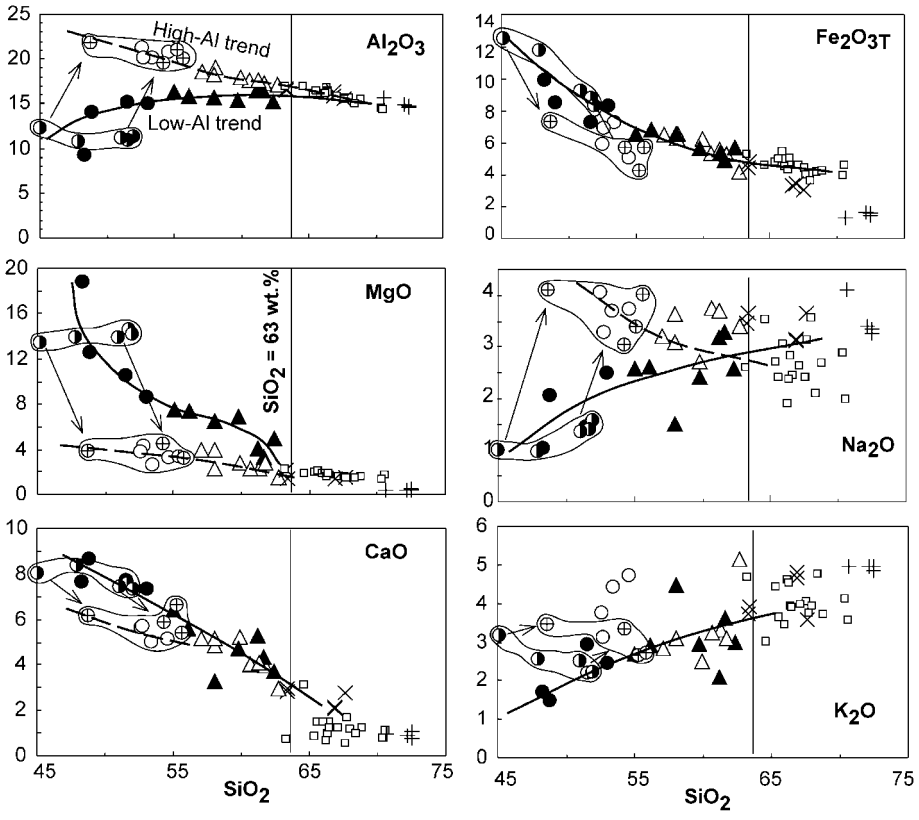

Fig. 10. Harker variation diagrams showing the main major element trends displayed by the rocks of the Sanabria complex (symbols as in Fig. 9). Lines show the main trends defined by these rocks: a high-Al trend (dashed line) and a low-Al trend (continuous line). The high-Al trend links monzodiorites and Bt-diorites with tonalites, granodiorites and migmatites. The low-Al trend links Hb-gabbros and Hb-diorites. The two trends converge at silica contents of ~63 wt % for most elements. Samples from the Garandones profile are plotted with different symbols: half-filled circles for Hb-gabbros and circles with crosses for the monzodiorites. Arrows link these two groups of rocks and indicate the direction of enrichment or depletion. Other symbols as in Fig. 9.

are listed in Table 3. Although the number of analyses is small and does not allow an in-depth study of the isotopic variation, the available data are useful for comparison with other appinitic complexes and provide some constraints on the petrogenetic hypotheses inferred from field relations and geochemical variations. The most salient feature is the steep trend in Nd–Sr isotope space defined by all rock types from gabbro to granite (Fig. 14); there is a narrow range in the initial Sr isotopic composition (at 345 Ma) and a wide variation in the initial Nd isotopic ratios, expressed as ε_{Nd} (345 Ma). This pattern is consistent with other appinitic complexes from the Iberian Variscan massif, such as the Vivero massif in Northern Spain (Galán *et al.*, 1996) and the Gredos batholith in Central Spain (Moreno Ventas *et al.*, 1995). It is remarkable that two samples of hornblende gabbro, which are nearly identical in terms of their major element chemistry and mineral assemblage, are very different in terms of their Nd isotope composition: one is close to a primitive, CHUR-like, composition ($\varepsilon_{Nd} \sim -1$) and the other is close to typical Variscan crustal values (Vivero and Gredos massifs) and granodiorites ($\varepsilon_{Nd} \sim -4$). Most of the mafic and intermediate rocks have a clear crustal signature in terms of Nd isotopic composition. Also for comparison, two samples of the Ollo de Sapo migmatitic gneisses were included in this study. These plot at the left end of the wide field in Sr initial ratios displayed by the gneisses in the Iberian massif (Beetsma, 1995; Castro *et al.*, 1999). The Sanabria samples roughly define a curvilinear trend that may approach an assimilation–fractional crystallization (AFC) trend. This aspect will be discussed further below.

DISCUSSION

Intrusion mechanisms and time sequence in relation to regional deformation

It has been shown previously that the main episode of magma intrusion appears to be coeval with the migmatization and penetrative deformation of the host rocks (Ollo de Sapo gneisses). The structures

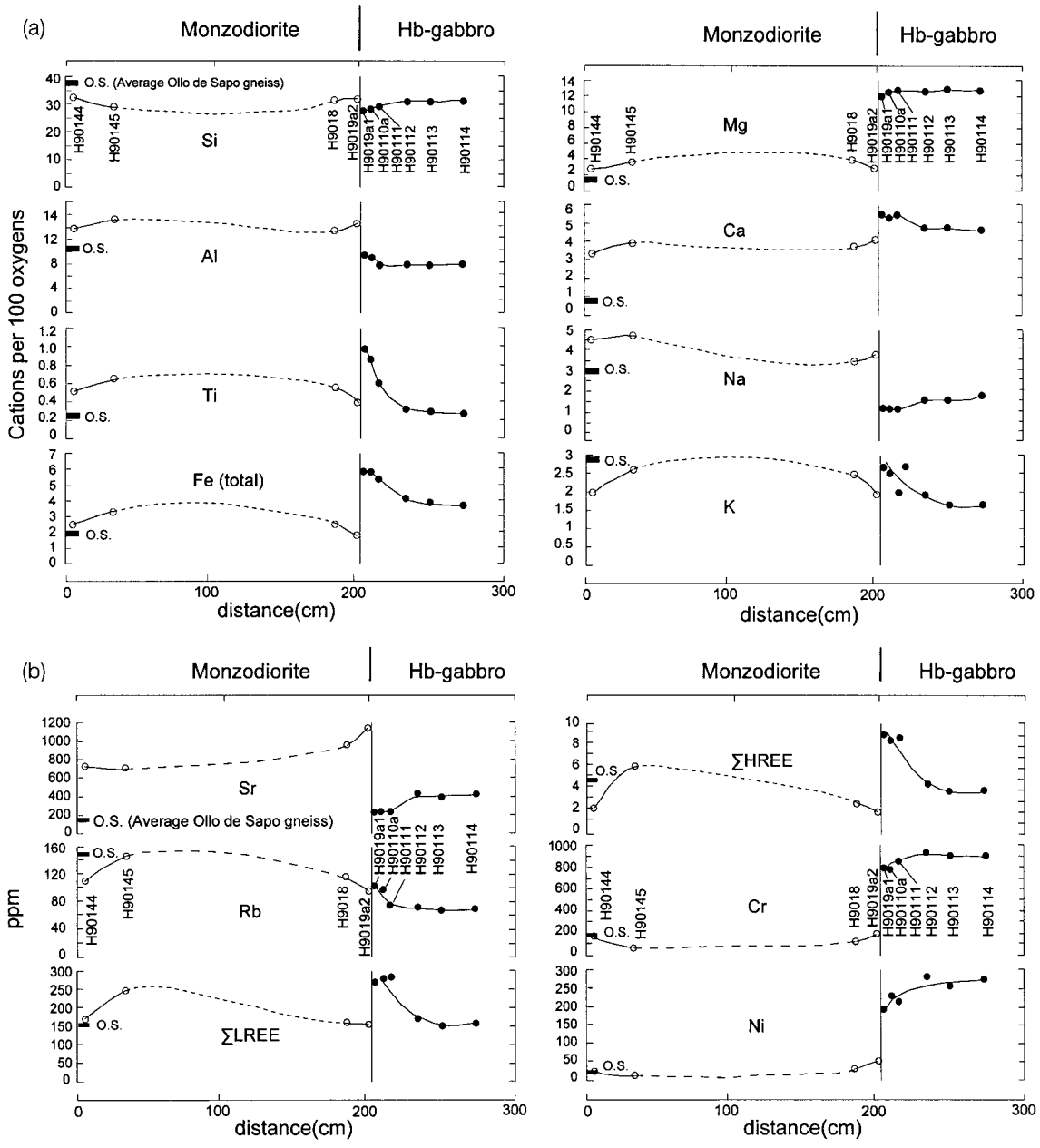

Fig. 11. Compositional profiles across the contact between Hb-gabbros and monzodiorites in the Garandones profile (sample locations in Fig. 7). The black box labelled O.S. on the ordinate represents the composition of the migmatitic gneisses (see text for further details).

developed during this deformational episode, here attributed to the regional D_2 phase, are affected by the D_3 folding episode, which is responsible for the reorientation to vertical of the D_2 fabrics (Fig. 2). If the D_2 structures are restored to their pre-D_3 position, they define a subhorizontal shear zone with a top-to-the-SE sense of movement. This phase is described as a SE-directed crustal extension in nearby sectors of the Central Iberian Zone (Escuder *et al.*, 1994; Díez Balda *et al.*, 1995). Experimental data on the melting relationships of the Ollo de Sapo gneiss (Castro *et al.*, 2000) indicate that migmatization of this gneiss took place by decompression melting, in agreement with the observed field relationships between D_2 structures and migmatization. However, it is worth mentioning that magma intrusion and migmatization conditions could have survived until the end of the D_3 episode, as revealed by small septa of leucogranitic bodies located at the southern part of the studied area, and by the structural and magnetic fabric study of

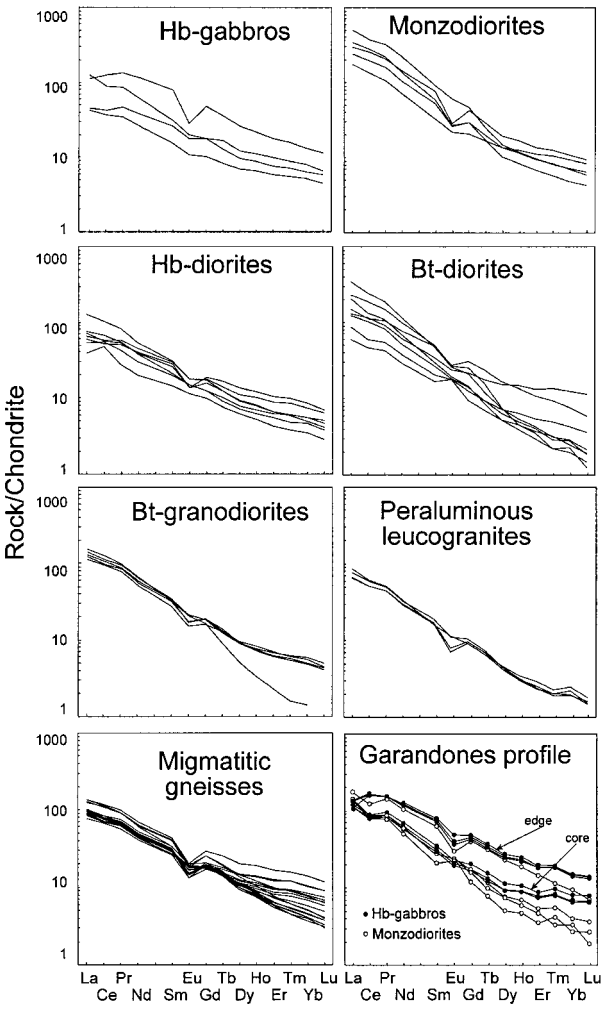

Fig. 12. Chondrite-normalized REE patterns [normalization according to Nakamura (1974)] for the rocks of the Sanabria complex.

Vegas *et al.* (2001). Decompression melting appears to be coeval with the intrusion of basic magmas into the anatectic zone. Thus, both processes, decompression and heating, may have contributed jointly in producing crustal anatexis in this sector of the Variscan orogen.

Identification of magmatic series and processes

Intermediate rocks

With regard to the intermediate rocks, the geochemical relationships observed in the Garandones Lake area are very informative about the range of processes that have occurred. The compositional variations displayed in the profiles of Fig. 11 exclude the possibility that these magma bodies were generated separately and one intruded into the other accidentally. Furthermore, the shape of the profiles cannot be the result of a geochemical gradient between two different magmas of contrasted compositions. In some cases the element increasing towards the contact, within the marginal part of the gabbro body, is depleted in the surrounding monzodiorite. This is the case for Ti, K and Fe (Fig. 11). Conversely, the elements decreasing towards the contact are enriched in the surrounding monzodiorite (e.g. Si). The zone of major variation, or compositional gradient, within the hornblende gabbro body is a narrow band that coincides with the zone with differences in grain size and modal abundances. This band is richer in biotite and the grain size is finer than in the interior of the mafic hornblende gabbro body. The interpretation of this band as a chilled margin is in agreement with the compositional variations recorded by biotite as discussed above. However, whole-rock variations in major and trace elements require more detailed attention. The compositional jump across the interface is independent of the compositional gradient observed within the narrow band of the gabbro body, as mentioned above. It is paradoxical that this narrow band crystallized earlier than the central part of the gabbro and at the same time it is enriched in incompatible elements such as K, Rb and the REE. The enrichment in K may be accounted for by the early precipitation of biotite in the margins of the mafic body. This is in agreement with the particular textural relations of these mafic rocks in which biotite is an early phase included within euhedral hornblende. Consequently, the potassic character of the mafic bodies is likely to be a primary feature inherited from their mantle source, not acquired during crystallization in the continental crust by assimilation of potassic rocks. A simple mixing calculation indicates that a mass fraction of ~40% of granite must be assimilated to produce the K content of these mafic magmas. This mass fraction implies a silica content in the resulting hybrid of ~60 wt %, and this is in disagreement with the low silica content (~50 wt %) of the gabbroic rocks with K_2O contents of ~2·5 wt %. A similar estimation is obtained from the REE content of these mafic rocks. A mass fraction of granite >50 wt % is necessary to account for the high content in REE, especially in LREE. The conclusion from these estimations is that the high contents of both K and REE cannot be accounted for by assimilation of granitic rocks alone. The basic magma that intruded into the anatectic rocks of the Sanabria complex was originally rich in K and REE as well as in water. Primary water is of fundamental importance in accounting for the geochemical features and field relations displayed by these appinitic complexes.

The enrichment in Rb in the marginal zones of the mafic bodies may be interpreted in the same way as

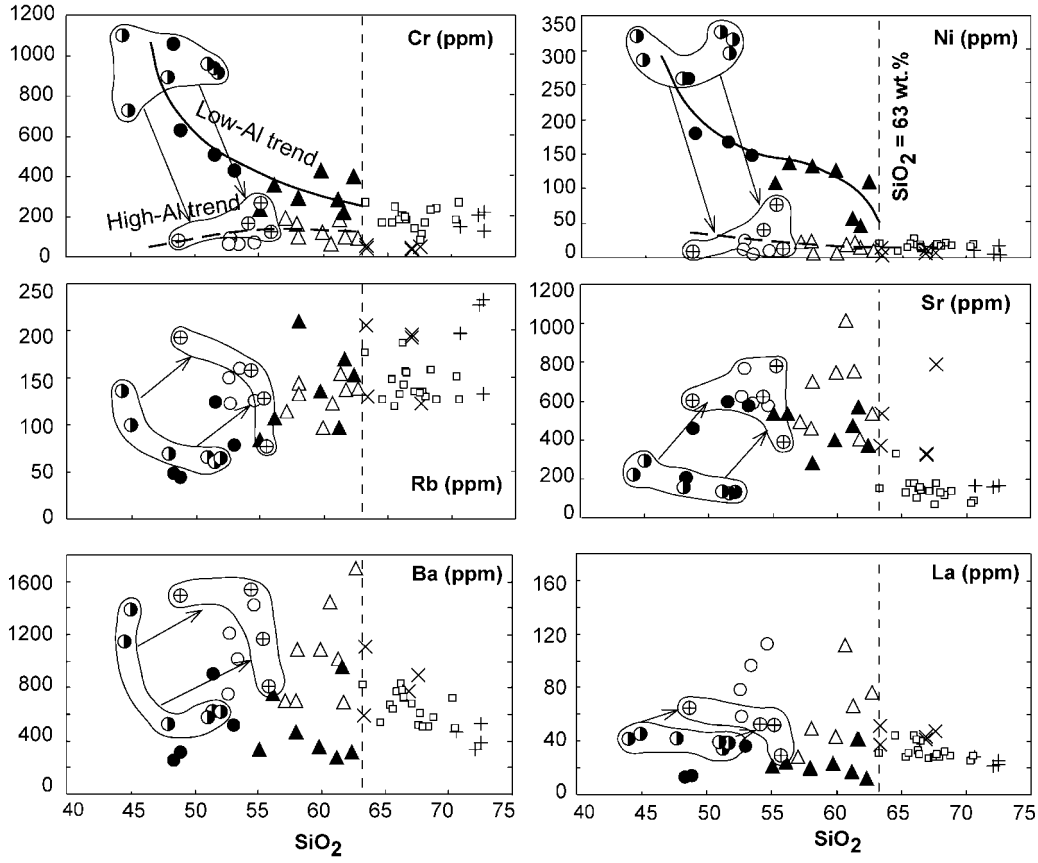

Fig. 13. Variation of selected trace elements vs SiO_2 content for representative rocks from the Sanabria complex. The main trends, the high-Al and low-Al trends distinguished on the basis of major elements, can also be traced for some compatible trace elements such as Cr and Ni. Rb, Sr and Ba show a scattered distribution. Samples surrounded by an outline correspond to the Garandones profile. Arrows linking Hb-gabbros and monzodiorites indicate trends of enrichment or depletion. Symbols as in Figs 9 and 10.

K because of the coupled behaviour of both elements. However, the enrichment in REE and the depletion in refractory elements such as Cr and Ni remain paradoxical. A possible explanation is that fluids released from the crystallizing mafic magma transported REE and other incompatible elements from the interior of the magma body towards the surroundings and altered the crystallizing chilled margin. This margin was relatively cooler and more crystalline than the interior of the mafic magma and may have acted as a trap for incompatible elements that were captured by crystallizing phases such as apatite and allanite that are very abundant in the marginal facies of the mafic bodies. The compositional jump observed across the interface is compatible with the separation of a discrete fluid phase. This may be a water-rich pegmatitic fluid that the basic (gabbro) magma released during crystallization within the migmatite host.

The pegmatitic textures, evidencing ion mobility assisted by a fluid phase, of the monzodiorites surrounding the mafic bodies are also in favour of this interpretation. The composition of this gabbro is in some way residual rather than a primary melt, based on the high MgO content (up to 18 wt %). The residual character may be related to the extraction of a water-rich fluid phase that is transferred to the migmatite host. The absence of migmatites in mutual contact with the mafic bodies indicates that the monzodiorites are likely to be the result of chemical reaction between a water-rich fluid released from the basic magma and the host migmatites. The geochemical variations for the HA trend in which the pegmatitic monzodiorites are included support this interpretation. The evolution of the LA trend may be related to a process of magmatic fractionation from the same basic magma.

In summary, a water-rich basic magma, rich in K and REE, intruded into an anatectic zone within the continental crust and underwent two different processes. One is related to crystal fractionation and the production of Al-poor intermediate magmas (the LA trend). The other is related to the release of a water-rich fluid towards the host migmatites that reacts with

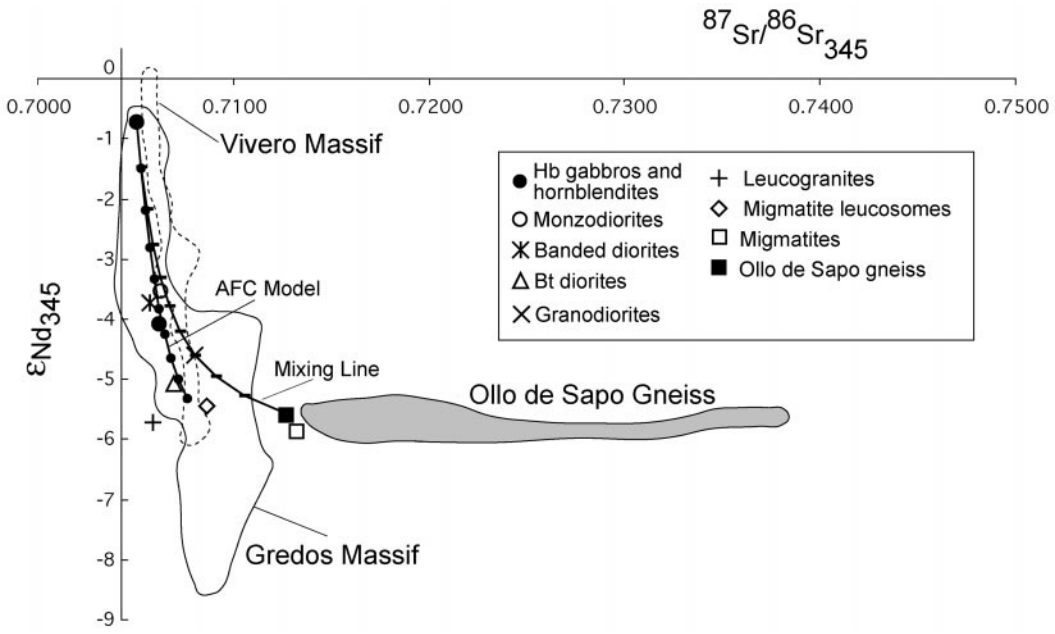

Fig. 14. Variation of $^{87}Sr/^{86}Sr$ vs ε_{Nd} at 345 Ma for representative samples from the Sanabria complex. The fields of the most representative rock types in the Gredos massif (Moreno Ventas *et al.*, 1995; Bea *et al.*, 1999) and in the Vivero massif (Galán *et al.*, 1996) are depicted for comparison. These are typical peri-batholithic appinite complexes of the Iberian massif. A model AFC curve is shown linking the more primitive basic rock and the Ollo de Sapo migmatites. Values of the partition coefficients used (D) are 1·2 for Nd and 0·51 for Sr (Sisson, 1994). The ratio of assimilation to fractional crystallization (r) is 0·5. A value of D for Sr <1 must be applied to fit data points to the model curve. A tentative value for D_{Sr} of 0·4 is taken. The behaviour of Sr as an incompatible element is in agreement with the observed enrichment in Sr in the pegmatitic monzodiorites surrounding the Hb-gabbros of Garandones. The model AFC departs from a simple mixing line in which no fractionation is considered ($D = 1$ for Sr and Nd), indicating that Sr fractionation is needed to account for the observed variations.

these peraluminous rocks and produces Al-rich intermediate magmas (the HA trend) of monzodiorite composition. Remnants of partially digested Ollo de Sapo migmatites included within the monzodiorites of the Garandones Lake area provide further support for this process of fluid-assisted reaction and assimilation. The process is, however, more complex, as denoted by the presence of plagioclase cumulates in patches within the monzodiorites surrounding the hornblende gabbros as mentioned above. These relations indicate that additional differentiation processes occurred during assimilation. These processes are compatible with the observation of a marked enrichment in Sr (>1000 ppm) within the monzodiorites. This enrichment is coupled with a similar enrichment in Na but not in Ca, which is retained in the Hb-rich cumulates. Other elements have concentrations intermediate between the composition of the mafic body and that of the Ollo de Sapo gneisses–migmatites (Fig. 11).

AFC modelling and implications

This complex process involving magmatic fractionation and, at the same time, water loss to the surrounding crustal rocks may produce a series of intermediate rocks that follow a hypothetical trend of AFC. The Sr and Nd initial isotopic ratios of the basic and intermediate rocks of the Sanabria complex (Fig. 14) display a curved trend close to the model curve of an AFC mixing model assuming an assimilation/fractionation ratio (r) of 0·5. For this model curve it is assumed that r and the partitioning coefficients (D) for Sr and Nd remain constant during the crystallization–assimilation combined process (DePaolo, 1981). It is interesting to note that Sr must be an incompatible element and Nd must have a D value close to unity for the model curve to be close to the data points (Fig. 14). This situation is not very usual in basaltic systems but may be important if amphibole, and not plagioclase, is the dominant fractionating phase (DePaolo, 1981). In the case of the Sanabria trend, the residual gabbroic rocks are dominantly composed of hornblende with subordinate plagioclase. At the same time, the monzodiorites surrounding the Hb-gabbros are richer in Sr than both the gabbro and the hosting migmatites (Fig. 11b), denoting that plagioclase was not an important fractionating phase in this system and that Sr was enriched in the residual fluids expelled from the water-rich basaltic magma; i.e. Sr behaves as an incompatible

element. This observation satisfies the requirement of the AFC modelling shown in Fig. 14. However, the simple process of a magma chamber that assimilates country rocks at the same time as it fractionates into a crystal cumulate, as required for AFC geochemical modelling (DePaolo, 1981), is not in agreement with field relations observed within the Sanabria complex. It seems plausible that the basic magma underwent hornblende fractionation as indicated by the low-Al trend of intermediate rocks and the richness in Hb of the more mafic gabbro. However, as denoted by field relations and geochemical variations in the Garandones profile, assimilation occurred between a fluid phase released from the crystallizing gabbro and the hosting migmatites. As Sr was partitioned to this fluid phase, the overall modelling is similar to an AFC process, implying the migmatites and gabbros as the end-members (Fig. 14). However, this process took place outside the magma chamber and involved a fluid phase that reacted with surrounding migmatites. This may be considered a special case of AFC in which fractionation is related to the separation of a fluid phase rather than to the fractionationation of crystals alone. It must be remarked that this situation is triggered by the crystallization within the continental crust of a water-rich basaltic magma. The operation of this special case of AFC may be the most usual one for subduction-related, water-rich basic magmas emplaced at any level into the continental crust; with the implication that many intermediate rocks with hybrid isotopic signatures may have their origin in the continental crust generated by processes of fluid-assisted assimilation and fractional crystallization.

Identification of the parental basic magma

The identification of a parental basic magma, as required for any petrogenetic modelling, is not straightforward. There is no unambiguous textural criterion that may be used to identify any rock of the Sanabria complex as crystallized from a primary melt. The parallel and steep REE patterns displayed by the monzodiorites and biotite diorites (Fig. 11) strongly suggest that they were not generated by a single process involving fractionation of a mineral phase such as hornblende alone. The comparison between the hornblende gabbros and the monzodiorites from the Garandones profile indicates that REE depletion occurred in the interiors of the gabbro bodies compared with the margins. As mentioned above, this enrichment in REE in the margins cannot be related to a compositional gradient associated with the proximity of the monzodiorite magma because the monzonites are poorer in REE than the gabbro margin. A plausible interpretation to account for these paradoxical variations is that REE were transported by a water-rich fluid released from the basic magma and were trapped by the crystallizing chilled margin. The enrichment in LREE may be related to such a process of fluid migration as a result of the preference of the LREE for water-rich fluids compared with heavy REE (Kogiso *et al.*, 1997). It is noteworthy that the hornblende gabbros are richer in REE and other incompatible elements than the migmatitic gneisses.

Initial Sr–Nd isotopic ratios of the Sanabria rocks are comparable with those of other peri-batholithic appinite complexes of the Iberian massif (Fig. 14). There is a strong heterogeneity in initial $^{143}Nd/^{144}Nd$ (ε_{Nd}) in contrast to a small variation in $^{87}Sr/^{86}Sr$ that is close to Bulk Earth values and much lower than the $^{87}Sr/^{86}Sr$ of the host gneissic rocks in the case of the Sanabria complex. It is noticeable that hornblende gabbros very similar in major-element composition and mineral assemblage have ε_{Nd} values that vary by 3ε units. This Nd isotope heterogeneity may be inherited from their mantle source. However, transport of REE in a fluid phase, as previously deduced from local variations between the hornblende gabbros and monzodiorites in the Garandones profile, may contribute to the observed isotopic heterogeneities. An important supply of REE from the hosting gneissic rocks may also account for the heterogeneous Nd isotope compositions of the resulting hybrids. The relatively low initial $^{87}Sr/^{86}Sr$ of the appinitic rocks is largely explained because most of the Sr is supplied to the system by the parent basic magma. This is true even for monzodiorites inferred to have formed by interactions between fluids released from the basic magmas and the hosting gneissic rocks. The fact that these mantle-derived basic magmas were rich in water, K, REE and other incompatible elements such as Rb, and at the same time have a low Sr initial isotopic ratio, may appear paradoxical.

Petrogenetic model

A simplified model of the processes involved in the generation of the Sanabria appinites is displayed in Fig. 15. The process may start with the invasion of a mid-crustal area composed of mica-rich volcanoclastic and metasedimentary rocks of the Ollo de Sapo formation by a hydrous basic magma (Stage I, Fig. 15). The source of this hydrous magma is most likely to be an enriched region of the lithospheric mantle in a supra-subduction zone environment. Crystallization of this hydrous magma within the continental crust may have occurred at pressures of the order of 6 kbar (Martínez *et al.*, 1990). As water solubility is highly dependent on pressure (Burnham, 1979), emplacement of the magma at this crustal level would

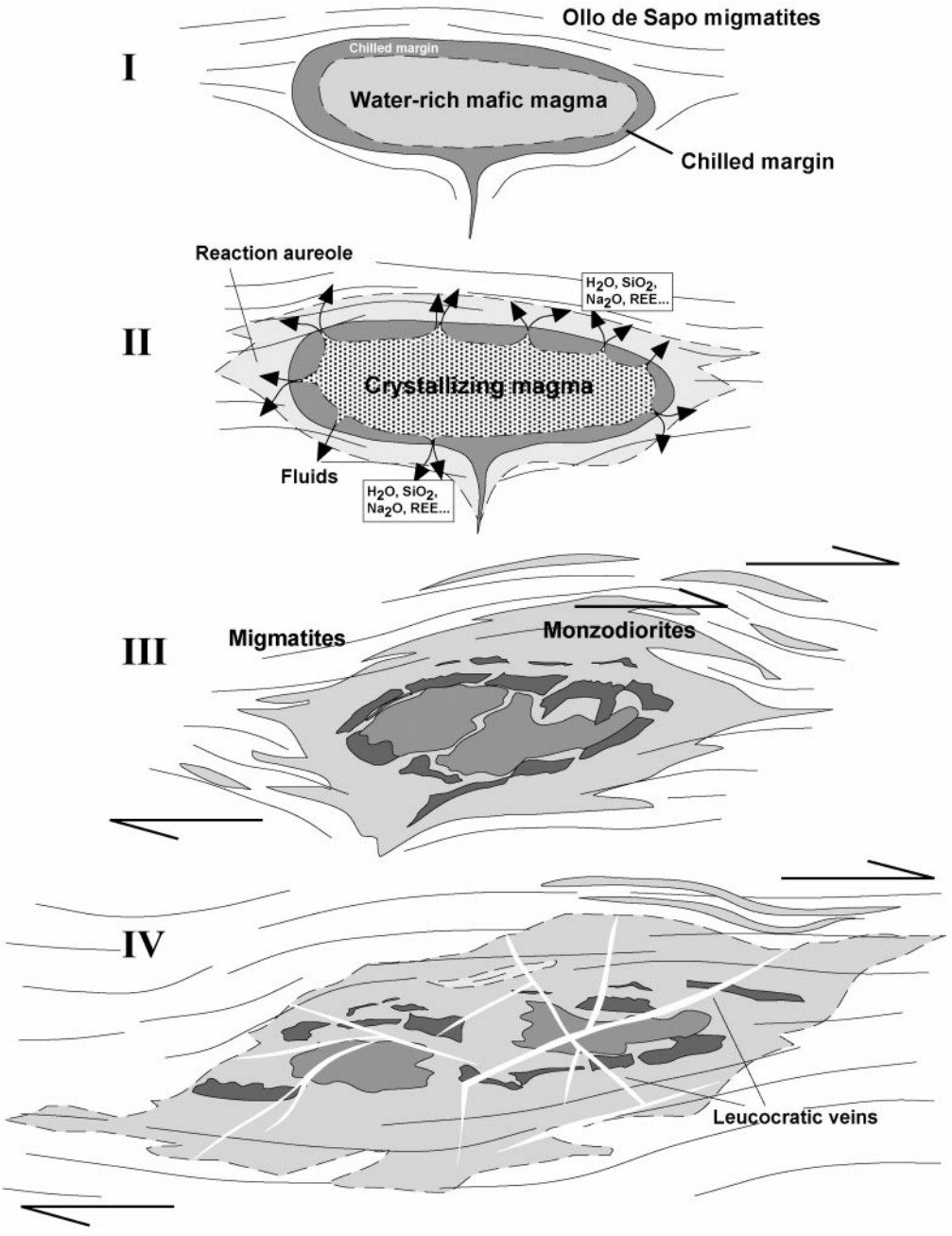

Fig. 15. Schematic illustration of the sequence of processes, ordered in a time sequence from I to IV, that were involved in the generation of the Sanabria appinite–migmatite complex, based on petrological and structural relationships. The formation of intermediate rocks, and possibly granodiorites, surrounding the basic intrusion is triggered by the release of a water-rich fluid from the basic intrusion towards the surrounding migmatites (see text for explanation).

eventually result in the release of significant amounts of water to the surrounding crust. The high solubility of alkalis and silica in this supercritical fluid (e.g. Grove *et al.*, 2002) makes it an important metasomatic agent, able not only to reduce the melting point of the surrounding rocks, but also to change the composition of the partial melts forming in the migmatites. At this stage (II, Fig. 15), a chilled margin may develop within the basic intrusion near the interface with the host migmatites. The water-rich fluid may pass through this chilled margin either by intergranular diffusion or along fractures. The passage of this fluid

is recorded by ionic interchange within the chilled margin as evidenced by the observed geochemical variations. It is interesting to note that a supposedly mobile element such as K is retained within the basic magma. The reason is that K is fixed during the early stages of magmatic crystallization by the Mg-rich biotite; this is an early mineral phase in these Mg- and K-rich magmatic systems. Consequently, the composition of the fluid phase released from the crystallizing basic magma may be dominated by H_2O, SiO_2 and Na_2O. As temperature falls and the basic magma begins to crystallize, the surrounding migmatites are fluxed by the water-rich fluids released from the mafic intrusion. At this stage (III, Fig. 15), significant amounts of monzodiorite magma may be developed in the migmatitic areas surrounding the mafic intrusion. The process may be facilitated if crystallization and fluid migration are occurring simultaneously with crustal thinning and extension. This is the case in the Sanabria complex, as deduced from the observed deformation fabrics. In this tectonic scenario, the minimum amount of water needed to generate a granite or monzodiorite melt in the aureole of the mafic intrusion is decreased as pressure decreases. The consequence is that individual crystals and enclaves may be dissolved in the silicate melt during decompression. The efficiency of this process has been proved by means of experimental studies (Castro *et al.*, 2002*b*). The contact relationships and shape of the hornblende gabbro small enclaves enclosed by the monzodiorites could be related to dissolution during decompression in a water-rich magma.

In the final stage (IV), the more mafic portions of the composite system (hornblende gabbros) are brecciated and back-veined (IV, Fig. 15) by leucocratic veins associated with the regional shearing that produced the banded, magmatic structures in the layered diorites and the intercalations of diorites within the migmatites surrounding the intermediate zones.

Granodiorites

The generation of the granodiorites is probably more complex; although the results of this study are not conclusive. According to experimental studies (Castro *et al.*, 1999, 2000), partial melting of the migmatitic rocks (the Ollo de Sapo gneisses) cannot produce the granodiorites either by fluid-present melting or by fluid-absent melting. Some additional Ca is necessary to generate granodiorites of the appropriate composition from the migmatites in the Sanabria area. Moreover, the granodiorites plot in a field intermediate between the monzodiorites and the migmatites. As granodiorites are hybrid rocks according to their Nd isotopic signatures, they may be viewed as resulting from some kind of further interaction between the monzodiorites and the migmatites (the Ollo de Sapo gneiss) hosting the mafic intrusions of Sanabria. This interaction may imply that granodiorites resulted from the partial melting of hybridized parts of the continental crust formed by alternations of monzodiorite and migmatite. This hypothesis provides a very attractive explanation for the complex field relations in the Sanabria massif, which do not favour a simple process of magma mixing or assimilation. Although granodiorites may result from partial melting of such a mixed source, as generated by the invasion of pelitic migmatites by basic magmas, there is no firm evidence to support this from the results of this study. The granodiorites are intrusive at this crustal level and show no transition with the other mafic and intermediate magmatic rocks of the area. If derived by melting of a mixed source, this must have occurred at deeper crustal levels than the present exposures of the Sanabria complex. Some support for this hypothesis is provided by the geochemical relationships between the granodiorites, diorites and pelitic migmatites.

CONCLUSIONS

The Sanabria complex shows unequivocal field relations between members of the appinitic suite and between these and migmatites derived by anatexis of local basement gneisses (Ollo de Sapo gneiss). These relations suggest a derivation of the monzodiorites and biotite diorites by fractionation and H_2O fluid-assisted melting of the crustal rocks surrounding the mafic intrusions. The hydrous basic magmas may be derived from an enriched region of the mantle associated with subduction. Reaction between fluids released from the crystallizing basic magma and the host migmatites was responsible for the generation in the crust of a diverse range of intermediate rocks in the Sanabria complex.

ACKNOWLEDGEMENTS

An early version of this paper benefited from critical comments by Ed Sawyer and an anonymous referee. We acknowledge financial support from Project BTE 2001-2769 of the Spanish Ministry of Science and Technology, from the Junta de Andalucía (Group RNM-120) and from the Huelva University.

REFERENCES

Arias, D., Farias, P. & Marcos, A. (2000). Structure and stratigraphic sequence of the Viana do Bolo–A Gudiña area: implications on the stratigraphic position of the Ollo de Sapo Formation (Ollo de Sapo Antiform, NW Spain). *15th International Conference on Basement Tectonics, Galicia 2000, A Coruña, Program with Abstracts*, pp. 199–201.

Bailey, E. B. (1960). *The Geology of Ben Nevis and Glen Coe*. Memoirs of the British Geological Survey, 2nd edn. London: British Geological Survey, 307 pp.

Bea, F., Montero, P. & Molina, J. F. (1999). Mafic precursors, peraluminous granitoids, and lamprophyres in the Avila batholith: a model for the generation of Variscan batholiths in Iberia. *Journal of Geology* **107**, 399–419.

Beetsma, J. J. (1995). The late Proterozoic/Paleozoic and Hercynian crustal evolution of the Iberian Massif, N Portugal as traced by geochemistry and Sr–Nd–Pb isotope systematics of pre-Hercynian terrigenous sediments and Hercynian granitoids. Ph.D. thesis, Vrije Universiteit Amsterdam.

Bowes, D. R. & McArthur, A. C. (1976). Nature and genesis of the appinite suite. *Krystalinikum* **12**, 31–46.

Burnham, C. W. (1979). Magmas and hydrothermal fluids. In: Barnes, H. L. (ed.) *Geochemistry of Hydrothermal Ore Deposits*. New York: Wiley–Interscience, pp. 71–136.

Capdevila, R. (1969). Le métamorphisme regional progressif et les granites dans le segment hercynien de Galice Nord Oriental (NW de l'Espagne). Ph.D. thesis, University of Montpellier.

Castro, A. (2001). Plagioclase morphologies in assimilation experiments. Implications for disequilibrium melting in the generation of granodiorite rocks. *Mineralogy and Petrology* **71**, 31–49.

Castro, A. & Stephens, W. E. (1992). Amphibole-rich polycrystalline clots in calc-alkaline granitic rocks and their enclaves. *Canadian Mineralogist* **30**, 1093–1112.

Castro, A., Patiño Douce, A. E., Corretgé, L. G., De La Rosa, J. D., El-Biad, M. & El-Hmidi, H. (1999). Origin of peraluminous granites and granodiorites, Iberian massif, Spain. An experimental test of granite petrogenesis. *Contributions to Mineralogy and Petrology* **135**, 255–276.

Castro, A., Corretgé, L. G., El-Biad, M., El-Hmidi, H., Fernández, C. & Patiño Douce, A. (2000). Experimental constraints on Hercynian anatexis in the Iberian Massif, Spain. *Journal of Petrology* **41**, 1471–1488.

Castro, A., Corretgé, L. G., De la Rosa, J. D., Enrique, P., Martínez, F. J., Pascual, E., Lago, M., Arranz, E., Galé, C., Fernández, C., Donaire, T. & López, S. (2002*a*). Palaeozoic magmatism. In: Gibbons, W. & Moreno, T. (eds) *The Geology of Spain*. London: Geological Society, pp. 117–153.

Castro, A., García Moreno, O., El-Hmidi, H. & Corretgé, L. G. (2002*b*). Dissolution of mafic microgranular enclaves by decompression melting in a water-saturated granitic magma. EMPG IX, ETH Zurich. *Journal of Conference Abstracts* **7**(1), 23.

Dallmeyer, R. C., Martínez Catalán, J. R., Arenas, R., Gil Ibarguchi, J. I., Gutiérez Alonso, G., Farias, P., Bastida, F. & Aller, J. (1997). Diachronous Variscan tectonothermal activity in the NW Iberian Massif: evidence from 40Ar/39Ar dating of regional fabrics. *Tectonophysics* **277**, 307–337.

Deer, W. A., Howie, R. A. & Zussman, J. (1966). *An Introduction to the Rock Forming Minerals*. Harlow: Longman, 528 pp.

DePaolo, D. J. (1981) Trace element and isotopic effects of combined wallrock assimilation and fractional crystallization. *Earth and Planetary Science Letters* **53**, 189–202.

Díez Balda, M. A., Vegas, R. & González Lodeiro, F. (1990). The Central Iberian Zone (autochthonous sequences): structure. In: Dallmeyer, R. D. & Martínez-García, E. (eds) *Pre-Mesozoic Geology of Iberia*. Berlin: Springer, pp. 172–188.

Díez Balda, M. A., Martínez Catalán, J. R. & Ayarza Arribas, P. (1995). Syn-collisional extensional collapse parallel to the orogenic trend in a domain of steep tectonics: the Salamanca Detachment zone (Central Iberian Zone, Spain). *Journal of Structural Geology* **17**, 163–182.

Escuder, J., Arenas, R. & Martínez Catalán, J. R. (1994). Tectonothermal evolution associated with Variscan crustal extension in the Tormes Gneissic Dome (NW Salamanca, Iberian Massif, Spain). *Tectonophysics* **238**, 117–138.

Fowler, M. B. & Henney, P. J. (1996). Mixed Caledonian appinite magmas: implications for lamprophyre fractionation and high Ba–Sr granite genesis. *Contributions to Mineralogy and Petrology* **126**, 199–215.

Fowler, M. B., Henney, P. J., Darbyshire, D. P. F. & Greenwood, P. B. (2001). Petrogenesis of high Ba–Sr granites: the Rogart pluton, Sutherland. *Journal of the Geological Society, London* **158**, 521–534.

French, W. J. (1966). Appinitic intrusions clustered around the Ardara pluton. *Proceedings of the Royal Irish Academy* **64B**, 303–322.

Galán, G. & Suárez, O. (1989). Cortlanditic enclaves associated with calc-alkaline granites from Tapia–Asturias (Hercynian Belt, NW Spain). *Lithos* **23**, 233–245.

Galán, G., Pin, C. & Duthou, J. (1996). Sr–Nd isotopic record of multistage interactions between mantle-derived magmas and crustal components in a collision context—the ultramafic–granitoid association from Vivero (Hercynian belt, NW Spain). *Chemical Geology* **131**, 467–491.

Galán, G., Corretgé, L. G. & Laurent, O. (1997). Low-potassium vaugnerites from Guéret (Massif Central, France). Mafic magma evolution influenced by contemporaneous granitoids. *Mineralogy and Petrology* **59**, 165–187.

Gebauer, D., Martínez-García, E. & Hepburn, J. C. (1993). Geodynamic significance, age and origin of the Ollo de Sapo Augengneiss (NW Iberian Massif, Spain). *AGU Annual Meeting, Boston, Abstracts with Programs*, p. A-342.

Gil Ibarguchi, J. I. (1980). Las vaugneritas de la región de Finisterre (Galicia, NW España). Probables productos de magmas anatécticos residuales. *Cuadernos do Laboratorio Xeológico de Laxe* **1**, 21–30.

Gil Ibarguchi, J. I. (1981). A comparative study of vaugnerites and metabasic rocks from the Finisterre region (NW Spain). *Neues Jahrbuch für Mineralogie, Abhandlungen* **143**, 91–101.

Grove, T. L., Parman, S. W., Bowring, S. A., Price, R. C. & Baker, M. B. (2002). The role of an H_2O-rich fluid component in the generation of primitive basaltic andesites and andesites from the Mt. Shasta region, N California. *Contributions to Mineralogy and Petrology* **142**, 375–396.

Holden, P., Halliday, A. N. & Stephens, W. E. (1987). Neodymium and strontium isotope content of microdiorite enclaves points to mantle input to granitoid production. *Nature* **330**, 52–56.

Julivert, M., Fontboté, J. M., Ribeiro, A. & Conde, L. N. (1974). *Memoria explicativa del Mapa Tectónico de la Península Ibérica y Baleares*. Madrid: IGME, 113 pp.

Kogiso, T., Tatsumi, Y. & Nakano, S. (1997). Trace element transport during dehydration processes in the subducted oceanic crust: 1. Experiments and implications for the origin of ocean islands basalts. *Earth and Planetary Science Letters* **148**, 193–205.

Lancelot, J. R., Allegret, A. & Iglesias Ponce de León, M. (1985). Outline of Upper Precambrian and Lower Paleozoic evolution of the Iberian Peninsula according to U–Pb dating of zircons. *Earth and Planetary Science Letters* **74**, 325–337.

Leake, B. E. (1978). Nomenclature of amphiboles. *Mineralogical Magazine* **42**, 553–563.

Le Maitre, R. W., Bateman, P., Dudek, A., Keller, J., Lameyre, J., Le Bas, M. J., Sabine, P. A., Schmid, R., Sorensen, H., Streckeisen, A., Woolley, A. R. & Zanettin, B. (1989). *A*

Classification of Igneous Rocks and Glossary of Terms. Oxford: Blackwell.

López Moro, F. J. (2000). Las rocas plutónicas calcoalcalinas y shoshoníticas del domo varisco del Tormes (Centro-Oeste español). Estudio mineralógico, geoquímico y petrogenético. Tesis Dotoral, Universidad de Salamanca, 441 pp.

Martínez, F. J., Corretgé, L. G. & Suárez, O. (1990). The Central Iberian Zone (autochthonous sequences): distribution, characteristics and evolution of metamorphism. In: Dallmeyer, R. D. & Martínez-García, E. (eds) *Pre-Mesozoic Geology of Iberia*. Berlin: Springer, pp. 207–211.

Martínez Catalán, J. R., Arenas, R., Díaz García, F. & Abati, J. (1997). Variscan accretionary complex of northwest Iberia: terrane correlation and succession of tectonothermal events. *Geology* **25**, 1103–1106.

Martínez García, E. (1969). Nota sobre la posición del 'Ollo de Sapo' en las provincias de Zamora y Orense (NW de España). *Comunicaçoes dos Serviços Geologicos de Portugal* **53**, 37–42.

Menendez, M. & Ortega, L. A. (1999). Evidence of magmatic hybridisation related with feeding zones: the synkinematic Guitiriz granitoids, NW Iberian Massif. In: Castro, A., Fernández, C. & Vigneresse, J. L. (eds) *Understanding Granites: Integrating New and Classical Techniques*. *Geological Society, London, Special Publications* **158**, 255–272.

Montero, P. & Bea, F. (1998). Accurate determination of Rb^{87}/Sr^{86} and Sm^{147}/Nd^{144} ratios by inductively coupled plasma mass spectrometry in isotope geoscience: an alternative to isotope dilution analysis. *Analytica Chimica Acta* **358**, 227–233.

Moreno Ventas, I., Rogers, G. & Castro, A. (1995). The role of hybridization in the genesis of Hercynian granitoids in the Gredos massif. Inferences from Sm/Nd isotopes. *Contributions to Mineralogy and Petrology* **120**, 137–149.

Nakamura, N. (1974). Determination of REE, Ba, Mg, Na and K in carbonaceous and ordinary chondrites. *Geochimica et Cosmochimica Acta* **38**, 757–773.

Navidad, M. (1979). Las series glandulares del sector central del Macizo Ibérico (Guadarrama centro-occidental). *Estudios Geológicos* **35**, 31–48.

Ortega, L. A. (1998). Estudio petrológico del granito sincinemático de dos micas de A Espenuca (A Coruña) Ph.D. thesis, Laboratorio Xeoloxico de Laxe, 380 pp.

Paterson, S. R., Vernon, R. H. & Tobisch, O. T. (1989). A review of criteria for the identification of magmatic and tectonic foliations in granitoids. *Journal of Structural Geology* **11**, 349–363.

Pin, C. & Santos Zalduegui, J. F. (1996). Sequential separation of light rare-earth elements, thorium and uranium by miniaturized extraction chromatography: application to isotopic analyses of silicate rocks. *Analytica Chimica Acta* **339**, 79–89.

Pin, C., Briot, D., Bassin, C. & Poitrasson, F. (1994). Concomitant separation of strontium and samarium–neodymiun for isotopic analysis in silicate samples, based on specific extraction chromatography. *Analytica Chimica Acta* **298**, 209–217.

Pitcher, W. S. (1997). *The Nature and Origin of Granite*. Glasgow: Chapman & Hall, 321 pp.

Pouchou, J. L. & Pichoir, F. (1984). A new model for quantitative X-ray microanalysis, Part I: application to the analysis of homogeneous samples. *La Recherche Aerospatiale* **3**, 167–192.

Sabatier, H. (1991). Vaugnerites, special lamprophyre-derived mafic enclaves in some Hercynian granites from Western and Central Europe. In: Didier, J. & Barbarin, B. (eds) *Enclaves and Granite Petrology*. Amsterdam: Elsevier, pp. 63–81.

Sisson, T. W. (1994). Hornblende–melt trace-element partitioning measured by ion microprobe. *Chemical Geology* **117**, 331–344.

Stephens, W. E. (2001). Polycrystalline amphibole aggregates (clots) in granites as potential I-type restite: an ion microprobe study of rare-earth distributions. *Australian Journal of Earth Sciences* **48**, 591–602.

Twiss, R. J. (1988). Description and classification of folds in single surfaces. *Journal of Structural Geology* **10**, 607–623.

Valverde, P. & Dunning, G. R. (2000). New U–Pb ages for Early Ordovician magmatism in Central Spain. *Journal of the Geological Society, London* **157**, 15–26.

Vegas, N., Aranguren, A. & Tubía, J. M. (2001). Granites built by sheeting in a fault stepover (the Sanabria Massifs, Variscan Orogen, NW Spain). *Terra Nova* **13**, 180–187.

Vernon, R. H. (1983). Restite, xenoliths and microgranitoid enclaves in granites. *Journal of Proceedings of the Royal Society of New South Wales* **116**, 77–103.

Vernon, R. H. (1991). Interpretation of microstructures of microgranitoid enclaves. In: Didier, J. & Barbarin, B. (eds) *Enclaves and Granite Petrology*. Amsterdam: Elsevier, pp. 277–291.